AFOSR-TR-94 0495

# REPORT DOCUMENTATION PAGE

| 2. REPORT DATE | 3. REPORT TYPE AND DATES COVERED |
|---|---|
| 29 April 1994 | Final<br>1 March 1990 - 30 September 1993 |

4. TITLE AND SUBTITLE

Mechanical Behavior and Flow Mechanisms in Refractory Metal Composites

5. FUNDING NUMBERS

G - AFOSR-90-0204
PE - 61103D
PR - 3484
TA - RS

6. AUTHOR(S)

I. Weiss and R. Srinivasan

7. PERFORMING ORGANIZATION NAME(S) AND ADDRESS(ES)

Mechanical and Materials Engineering Department
Wright State University
Dayton, OH 45435

8. PERFORMING ORGANIZATION REPORT NUMBER

9. SPONSORING/MONITORING AGENCY NAME(S) AND ADDRESS(ES)

AFOSR/NA
110 Duncan Avenue, Suite B115
Bolling AFB, DC 20332-0001

10. SPONSORING/MONITORING AGENCY REPORT NUMBER

11. SUPPLEMENTARY NOTES

12a. DISTRIBUTION/AVAILABILITY STATEMENT

Approved for public release, distribution in unlimited.

12b. DISTRIBUTION CODE

13. ABSTRACT (Maximum 200 words)

This report clearly demonstrates that the mechanical behavior of a refractory metal based composite, such as Nb-10 a/o Si alloy, can be improved considerably by tailoring the microstructure through thermomechanical processing (TMP). This desired microstructure consists of a fine grain silicide matrix reinfored with polygrain Nb particles which are elongated, oriented and aligned in a direction transverse to crack propagation. The powder processing route can achieve a fine grain structure which would exhibit high strength. But, significant improvements in fracture toughness would probably not be possible because factors such as the elongation, alignment, and orientation of the ductile reinforement phase are critical and provide additional energy absorption mechanisms such as pull-out, interface sliding, and crack bridging. The directional solidification (DS) process can produce a composite with reinforcing phase particles of specific size, spacing, and orientation. However, in the DS material, both the matrix and the ductile particles have single grain structures, which are prone to cleavage. Therefore, TMP by hot extrusion of a DS material will result in a composite with optimum properties.

14. SUBJECT TERMS

Niobium, silicide, composite, directional solidification

15. NUMBER OF PAGES

50

| 17. SECURITY CLASSIFICATION OF REPORT | 18. SECURITY CLASSIFICATION OF THIS PAGE | 19. SECURITY CLASSIFICATION OF ABSTRACT | 20. LIMITATION OF ABSTRACT |
|---|---|---|---|
| Unclassified | Unclassified | Unclassified | Unlimited |

NSN 7540-01-280-5500



Standard Form 298

# FINAL REPORT

| | |
|---|---|
| Project Title: | Mechanical Behavior and Flow Mechanisms in Refractory Metal Composites |
| Grant No.: | AFOSR-90-0204 |
| Investigators: | I. Weiss and R. Srinivasan<br>Mechanical and Materials Engineering Dept.<br>Wright State University<br>Dayton, Ohio 45435. |
| Project Duration: | March 1, 1990 - September 30, 1993 |
| Submitted to: | Dr. Alan H. Rosenstein, Program Manager<br>Air Force Office of Scientific Research<br>AFOSR/NC<br>110 Duncan Avenue, Suite B115<br>Bolling Air Force Base, DC 20332-0001 |



Dr. I. Weiss

Dr. R. Srinivasan

# INTRODUCTION

Materials for applications at temperatures in excess of 1200°C must exhibit a balance of strength, fracture toughness, microstructural, chemical and mechanical stability, and creep, oxidation, and fatigue resistance over a wide range of temperatures. Advanced metal-matrix composites based on refractory metal alloy systems are attractive because their high melting point give them the potential for high strength, stiffness and creep resistance. Figure 1, which shows a comparison of operating temperature versus strength-to-weight ratio for various classes of materials, illustrates the potential advantage that silicide matrix composites (SMC) have over conventional titanium and nickel alloys, metal-matrix-composites (MMC), and intermetallic-matrix-composites (IMC)[1,2]. The use of SMC's can reduce turbine air cooling, reduce the engine weight, and produce more efficient fuel combustion due to higher operating temperature. But, due to the brittle nature of the silicide matrix, the room temperature fracture toughness of this class of materials is inherently poor. So, the challenge lies in improving the room temperature fracture toughness without sacrificing much of the high temperature properties. Various SMC's based on systems such as Mo-Si ($MoSi_2$), Nb-Si ($Nb_5Si_3$, $Nb_3Si$), Cr-Si ($Cr_5Si_3$), W-Si ($WSi_2$), Ta-Si ($TaSi_2$, $Ta_5Si_3$) etc., have been considered [3,4,5].

Improving the toughness of a silicide by distributing a ductile phase within the brittle silicide matrix offers a promising solution to the problem. The concept of ductile phase toughening has been discussed extensively in literature [6-11]. Improvements in toughness result from a number of mechanisms, such as crack-bridging, crack-blunting, and crack-deflection. One or more of these mechanisms may act simultaneously in any given system to provide an overall improvement in toughness.

The Nb-Si system was chosen for this study based on earlier investigations [3]. Figure 2 shows a recent phase diagram of the Nb-Si system [12]. Hypo-eutectic compositions in this alloy system are examples of in-situ ductile phase toughened composites which are materials that solidify as a mixture of a brittle intermetallic matrix phase ($Nb_5Si_3$) with a distributed terminal metallic phase (Nb). Consider Nb-10 a/o Si, a typical alloy in this composition range. Upon slow cooling this alloy from the liquid state, pro-eutectic or primary Nb dendrites are the first to solidify, followed by a eutectic reaction occurs at 1920°C, forming $Nb_3Si$ and eutectic or

secondary Nb phases. The $Nb_3Si$ intermetallic compound decomposes by a eutectoid reaction to $Nb+Nb_5Si_3$ at 1770°C. At equilibrium, the phases present at room temperature in the Nb-10 a/o Si alloy are a hard silicide ($Nb_5Si_3$) phase and the terminal metallic Nb phase. However, the eutectoid reaction is extremely sluggish [13], and under the cooling rates observed in casting, this reaction is suppressed and the $Nb_3Si$ phase is observed at room temperature.

In any ductile phase toughened system, the distribution and morphology of the ductile phase play significant roles in determining the increase in toughness. Previous studies had suggested that some of the hypoeutectic Nb-Si alloys can be extruded at temperatures above 1450°C[3]. The extruded material showed considerably higher fracture toughness than the cast alloy. This study uses Nb-10 a/o Si as a model material to study the affect of thermomechanical processing on the microstructure, strength and fracture toughness of in-situ ductile phase toughened systems.

This final report brings together the results of the last year of the project and important results of previous years' work. The report has been written in the form of a paper, and will be submitted, with minor modifications, for peer review and publication. Details on many aspects, not specifically included in this report, can be found in prior reports, Masters' theses, and article preprints and reprints, which have been submitted during the course of the project.

## MATERIALS AND EXPERIMENTAL PROCEDURE

Two compositions of Nb-Si alloys were selected for this study. A hypoeutectic composition, Nb-10 a/o Si, representing a ductile phase toughened composite, and the eutectic composition, Nb-18.7 a/o Si, representing the matrix in the Nb-10 a/o alloy. Ingots of these nominal compositions were prepared by arc melting a master alloy in a water cooled copper crucible. The master alloy was prepared from double arc melted high purity Nb and electronic grade Si. The ingots were cooled in a controlled manner from the melt to minimize cracking. Chemical analysis revealed that the silicon content in the Nb-10 a/o Si ingots was 9.08 a/o, about 1 a/o less than the desired Si level. The carbon content varied from 0.10 to 0.2 a/o, and the O and N levels and they were found to be about 0.081 and 0.0465 a/o respectively.

Billets machined from the cast ingots were canned in molybdenum and extruded at 1800°C. The molybdenum can was removed, and some of the extruded material was re-canned and re-extruded at 1750°C. A nominal extrusion ratio of 4:1 was used for all extrusions, and a slow cooling was adopted after extrusion by placing the extruded material in a bed of insulating material. The conditions for hot extrusion were determined based on processing maps developed for the alloy [14]. Figure 3 is a summary of the processing maps, showing the boundary in the temperature-strain rate regime above which uniform deformation of the alloy was obtained during uniaxial compression.

In the as-cast condition (AC or I-Gen.), the microstructure consists of large primary Nb dendrites (light phase) in a continuous brittle $Nb_3Si$ matrix (dark phase), as seen in Figure 4(a). The eutectic, or secondary Nb phase is present as particles distributed in the $Nb_3Si$ matrix. Each primary Nb dendrite is a single large grain, as no high angle grain boundaries were observed in them. High angle grain boundaries were present in the $Nb_3Si$ phase. The location of these grain boundaries, indicated by cusps along the Nb/$Nb_3Si$ boundary seen in the SEM micrograph, was confirmed by TEM [15]. Following extrusion with a 4:1 area reduction at 1800°C both the primary Nb dendrites and $Nb_3Si$ phase are elongated and aligned in the extrusion direction (Fig 4(b)). The secondary Nb particles were not significantly affected by the extrusion. Varying contrast in the primary Nb phase caused by electron channeling indicates recrystallized Nb grains at different orientations. Energy dispersive x-ray analysis revealed that the silicide phase had a

composition of 75 a/o Nb and 25 a/o Si. Eutectoid decomposition of $Nb_3Si$, therefore, had not occurred after extrusion. TEM observations revealed that the $Nb_3Si$ phase had also recrystallized [16]. After re-extrusion at 1750°C the primary Nb particles are further elongated, oriented, and aligned in the extrusion direction (Fig. 4(c)). Again, the silicide phase was determined to be $Nb_3Si$. Further grain refinement was observed in both the Nb and $Nb_3Si$ phases. Table I and Figure 5 summarize the quantitative microstructural parameters for the different generations of the alloy. There is a decrease in the grain size of both Nb and $Nb_3Si$ phases, as well as a decrease in the particle size and inter particle spacing of the primary Nb phase perpendicular to the extrusion direction and in increase in the aspect ratio of the primary Nb phase particles [17].

Some of the specimens were vacuum annealed ($10^{-6}$ torr ) at 1450°C for 25 hours to transform the metastable $Nb_3Si$ to the stable $Nb_5Si_3$ phase. In all the annealed specimens, almost complete decomposition of $Nb_3Si$ to $Nb_5Si_3$ and Nb had occurred. Figures 6 (a) and (b) show the microstructure of the once and twice extruded materials after heat treatment (E1+HT and E2+HT). The black phase is $Nb_5Si_3$, while the lighter phase is Nb. Due to deposition of Nb during the eutectoid decomposition, both the pro-eutectic (primary) and eutectic (secondary) Nb particles appear to have coarsened.

Notched 4-point bending specimens of nominal dimensions 5 mm (t) x 10 mm (w) x 45 mm (L) were made by EDM from the as-cast and extruded billets to evaluate the fracture toughness. A notch of 5 mm in length and 0.2 mm in thickness was machined by EDM wire in all the fracture toughness specimens. Since the notch tip was rounded, and not the V-shaped and pre-cracked by fatigue, required by ASTM Standard E399 [18], the results of tests on these specimens are reported as $K_Q$ and not $K_{IC}$. Smooth 3-point bend specimens of dimensions 3 mm (t) X 4 mm (h) X 45 mm (L) were also made by EDM. The specimens made by EDM were ground to the specifications recommended by the MIL-STD-1942 [19].

Bend test jigs were made out of stainless steel and TZM for room temperature and high temperature tests, respectively. Fracture toughness was determined using four point bend tests, and fracture and yield strengths were determined using three point bend tests. Test were conducted at a constant speed of 0.254 mm/min (0.01" /min) over the temperature range of 25° to 1200°C. The peak load or the fracture load or the yield load was determined from the load-stroke data which was recorded on a digital storage oscilloscope. This measured load was then

used in the appropriate equation specified by MIL-STD-1942 (MR) or ASTM standard E399 to calculate the fracture toughness ($K_Q$) or bend strength ($\sigma_f$ or $\sigma_y$). Bend strength was calculated using the equation :

$$\sigma = \frac{3PL}{2bh^2} \tag{1}$$

where $\sigma$ is the yield strength ($\sigma_y$) or fracture strength ($\sigma_f$); P is the load at yield ($P_y$) or fracture ($P_f$); L is the load span; b is the specimen thickness; and h is the specimen height. Yield strength was calculated from the load at which the load-displacement curve deviated from a straight line, and fracture strength was determined from the load at which the specimen failed. Under certain test conditions, 3-point bend specimens, rather than undergoing fracture, deformed to an extent that their ends would come in contact with the jig and thus loading the jig. No fracture stress was recorded for such tests.

The fracture toughness $K_Q$ was calculated using the following equation [20].

$$K_Q = \frac{6Ma^{1/2}}{bw^2} f\left(\frac{a}{w}\right) \tag{2}$$

where, M is the applied bending moment at fracture and is given by (PL/2); P is the load at fracture; L is the load span; a is the notch length; b is the specimen thickness; w is the specimen width; and, *f(a/w)* is given by

$$f\left(\frac{a}{w}\right) = 1.99 - 2.47\left(\frac{a}{w}\right) + 12.97\left(\frac{a}{w}\right)^2 - 23.17\left(\frac{a}{w}\right)^3 + 24.8\left(\frac{a}{w}\right)^4 \tag{3}$$

## RESULTS AND DISCUSSION

### Three Point Bend Strength Tests

Smooth bend bars prepared from all three conditions i.e., AC, E1 and E2 of the alloy were tested on a three point bending jig at different temperatures ranging from 25° to 1200°C. The measured yield and fracture stresses at all the conditions tested are listed in Table II. Figure 7 shows the bend strength of Nb-$Nb_3Si$ composite as a function of temperature. At room temperature, fracture stress ($\sigma_f$) values are reported since very little plasticity was observed. Only yield stress values are plotted at all other temperatures. All three generations (AC, E1 and E2) of Nb-10 a/o Si alloy in the Nb + $Nb_3Si$ condition failed in a brittle manner at room temperature. The fracture strength increased from 334 MPa in the as-cast condition to 795 MPa in the E1 condition and further to 1344 MPa in the E2 condition. The strength of the alloy generally decreases with increasing temperature. Nb-10 a/o Si alloy under all thermomechanical conditions (AC, E1, E2) exhibited appreciable plastic deformation at 1000°C and 1200°C. The as-cast specimens at those temperatures yielded and then underwent fracture. Whereas specimens of the E1 and E2 material continued to bend without fracture until they had bent to such an extent that their ends came in contact with the jig.

Figure 8 shows the 3 pt. bending strength of Nb-10 a/o Si alloy in the heat treated condition. The fracture stresses measured for the E1 and E2 material at this condition were 512 and 806 MPa, respectively, and the corresponding yield stress values were 700 and 1188 MPa. Specimens of E1+HT and E2+HT materials did not fail above room temperature. Again, the bend strength was generally observed to decrease with increase in temperature for both E1+HT and E2+HT materials. It can be observed that the Nb-10 a/o Si alloy with the metastable $Nb_3Si$ phase matrix has higher bending strength than the composite with the stable $Nb_5Si_3$ phase matrix, except for the re-extruded material tested at 1200°C.

### Four Point Fracture Toughness Test

Fracture toughness was evaluated by bending a notched specimen in a four point bending

jig at different temperatures ranging from 25° to 1200°C. Since a non-standard notch geometry was used for these tests, the reported values are $K_Q$ and not $K_{IC}$. Table III and Figure 9 present the experimental fracture toughness values for the various testing conditions. At room temperature, the fracture toughness $K_Q$ of the Nb-10 a/o Si alloy in the AC condition was measured to be in the range of 11 to 15 MPa$\sqrt{m}$. Upon extrusion (E1) this value increases to 21.4 MPa$\sqrt{m}$, and after re-extrusion (E2), the fracture toughness increases further to 27.0 MPa$\sqrt{m}$. With increasing temperature, there is an increase in fracture toughness of all conditions of the alloy up to 1000°C, beyond which the fracture toughness drops off. The increase in toughness with temperature is attributed to an increase in ductility of both Nb and silicide phases. The drop in toughness at 1200°C is due to a significant decrease in the strength of the alloy. The highest measured fracture toughness was for the E2 material at 1000°C. Fracture toughness values of Nb-10 a/o Si in the heat treated condition ($Nb_5Si_3$ matrix) are presented in Figure 10. Here again the alloy in E2+HT condition offers the highest fracture toughness when compared to E1+HT and AC+HT. A $K_Q$ value of 25 MPa$\sqrt{m}$ was measured for the E2+HT material at room temperature. The fracture toughness decreases above 1000°C in a manner similar to the Nb + $Nb_3Si$ composite. Finally, the as-cast and the extruded composites with $Nb_3Si$ phase matrix (AC, E1 and E2) have greater fracture toughness values than the AC+HT, E1+HT, and E2+HT composites with $Nb_5Si_3$ matrix.

Figure 11 summarizes the effect of thermomechanical processing on both fracture toughness and bend strength. This figure shows that at all temperatures, fracture toughness increases linearly with bend strength. At room temperature a change in fracture toughness from about 13 to 27 MPa$\sqrt{m}$ for the Nb+$Nb_3Si$ composite is associated with a large change in strength from about 334 to 1344 MPa. At 1000°C, a change in yield strength from 356 to 638 MPa is associated with a much larger change in fracture toughness from about 18.8 to 49.1 MPa$\sqrt{m}$. At 1200°C also, small changes in strength result in large changes in fracture toughness.

**Fractography**

A small area of the fracture surface of the as-cast material is shown in Figure 12. The fracture surface is essentially flat and the crack appears to have swept through this area causing

brittle cleavage fracture of most of the large primary Nb particles and the silicide $Nb_3Si$ matrix. There are few primary Nb particles which have undergone ductile fracture. Extensive river patterns or ridge markings are observed in the primary Nb particles. Figure 13 shows an example of a crack passing through the silicide between two primary Nb particles. In general, the silicide matrix ($Nb_3Si$) does not show river patterns on their fracture surfaces. However, a few microcracks are observed in the silicide matrix. The fine speckle pattern seen in the $Nb_3Si$ phase is due to the secondary or eutectic Nb particles which have undergone ductile failure and have been pulled to "knife edges."

A small area of the fracture surface in the twice extruded (E2) material tested at room temperature is shown in Figure 14. This fractograph clearly reveals that the fracture surface is not flat and the crack appears to have changed its path many times, since the fractured Nb particles do not appear to be in the same orientation. A number of microcracks can be seen in the silicide phase. In addition, a large number of Nb particles have undergone ductile fracture after removal of constraints either by debonding from the matrix. These particles typically exhibit a dimpled surface, as shown in Figure 15.

**Bend Strength**

Thermomechanical processing of the Nb-10 a/o Si alloy results in changes in the morphology of the Nb and $Nb_3Si$ phases. In conjunction with these changes is an increase in the bend strength of the alloy. If the law of mixtures (equal strain hypothesis) is applicable to this in-situ composite, the strength of the composite can be expressed as:

$$\sigma_c = f_{Nb}\sigma_{Nb} + f_{Nb_3Si}\sigma_{Nb_3Si} \qquad (4)$$

where $f_{Nb}$ and $f_{Nb3Si}$ are the volume fractions, and $\sigma_{Nb}$ and $\sigma_{Nb_3Si}$ are the yield or fracture strengths of the two phases. At room temperature, the tensile strength of Nb is approximately 275 MPa [21], and for this alloy, with $f_{Nb}$= 0.68, the strength in the twice extruded condition is 1344 MPa. Therefore, though the Nb phase makes up the majority of the volume of the composite, its contribution to the strength is less than 15%. At elevated temperatures, the strength contribution of the Nb decreases further. At 1200°C, the strength of Nb phase is less than 40 MPa [21], and

provides only about 5% of the strength of the composite. With the major contribution to composite strength coming from the $Nb_3Si$ phase, one can expect that the changes in the strength of the composite will be most significantly affected by factors affecting the strength of the $Nb_3Si$ phase. Theories based on dislocation density predict that the strength of alloys increases with decreasing grain size.

$$\sigma = \sigma_0 + Kd^{-n} \tag{5}$$

where the exponent n has values between 1/2 and 1. One commonly observed relationship is the Hall-Petch relationship [22] where n = 1/2.

In the case of the Nb-10 a/o Si composite, the strength can be modeled as the following function of the grain size in the $Nb_3Si$ phase:

$$\sigma_c = f_{Nb_3Si}\left(\sigma_{0_{Nb_3Si}} + K_{Nb_3Si}\, d_{Nb_3Si}^{-n}\right) \tag{6}$$

where $\sigma_C$ is the fracture strength at room temperature or yield strength at elevated temperature. Figure 16 shows that the strength of this composite can be modeled as a function of the grain size in the $Nb_3Si$ phase with n = 0.75.

The data in Tables I and II show that the strength of the composite also increases with decreasing Nb grain size. But since the contribution of the Nb phase to the strength of the composite is small, this effect is probably only coincidental.

Figure 17 shows a comparison of the strength of Nb-10 a/o Si and Nb-18.7 a/o Si alloys in the E1 condition. The Nb-18.7 a/o Si alloy has the eutectic composition, and forms the matrix of the Nb-10 a/o Si alloy. At room temperature, the Nb-18.7 a/o Si alloy has a fracture strength of almost 2200 MPa, showing that the continuous $Nb_3Si$ is extremely strong. The Nb-10 a/o Si alloy has, in addition to the eutectic matrix, about 47 vol. percent of primary Nb particles. Since the Nb phase is considerably softer than the $Nb_3Si$ phase, the strength of the Nb-10 a/o Si is less than that of the Nb-18.7 a/o Si alloy.

## Fracture Toughness

The fracture toughness of a material is a measure of the energy required to fracture an alloy. The strain energy release rate $\zeta_R$ during fracture is related to the fracture toughness $K_Q$ through the equation

$$\zeta_R = \frac{K_Q^2}{E} \tag{7}$$

For a given specimen, notch, and loading geometry, the fracture toughness $K_Q$ is given by

$$K_Q = \sigma \cdot \sqrt{\pi a} \cdot f\left(\frac{a}{w}\right) \tag{8}$$

where $\sigma$ is the average stress on the cross section of the specimen at fracture, $a$ is the notch length and $f(a/w)$ is the geometry parameter given in Eq. 3. For a given specimen, notch, and loading geometry, Eq. 8 indicates that the fracture toughness increases linearly with the applied stress at fracture. This behavior is contrary to the general experience with metals and alloys in which increases toughness are associated with decreases in strength. However, in ceramics and other materials with limited ductility increases in toughness and strength are directly related [23].

Figure 18 shows the load, normalized by the cross-sectional area of the test specimen, versus displacement curves for four-point bend tests on the AC, E1, and E2 materials at room temperature. As the normalized load to fracture increases, the area under the load-displacement curve, which is the normalized work required to fracture the specimen, also increases, i.e., the toughness of the material is higher. This result shows that the microstructural modifications due to thermomechanical processing have resulted in an increase in the total work of fracture, and a concomitant increase in the fracture toughness $K_Q$. Figure 11 shows the relationship between $K_Q$ and the bending strength for the various microstructural modifications of Nb-10 a/o Si alloy. At each temperature, there is a linear trend between the two properties. The slope of the trend lines decreases with increasing temperature, indicating that small increases in strength at an elevated temperature results in significant toughness increases. These observations can be explained as follows:

The strain energy release rate during fracture $\zeta_R$, can be considered to be made up of several factors:

$$\zeta_R = \frac{K_Q^2}{E} = 2[W_S + W_{db} + W_{mc}] + A\int_0^{\epsilon} \sigma d\epsilon = 2W_F + A\int_0^{\epsilon} \sigma d\epsilon \qquad (9)$$

where, $W_S$ is the energy required to create the primary fracture surface; $W_{db}$ is the energy spent in debonding around the primary Nb particle; and $W_{mc}$ is the energy spent in causing microcracking in the silicide matrix. These three energy terms have been combined into a single term, $W_F$, the work of fracture. The last term is the energy required to plastically deform the ductile Nb phase, i.e., the ductile phase toughening term. In brittle materials, cracks will propagate if the elastic strain energy released during crack propagation becomes equal to the energy required to create the fracture surfaces [22]. If the energy required to extend a crack, the strain energy release rate, is increased, the fracture toughness of the material increases. Therefore, in simple terms, increases in any of the energy terms in Eq. 9 result in an increase in the fracture toughness of a composite. For example, during crack propagation, if the crack tip meanders or branches, the energy required to create the fracture surface $W_S$ increases. Similarly, the debonding at interfaces between phases in a composite, and the formation of secondary microcracks in the matrix expend energy ($W_{db}$ and $W_{mc}$), thereby increasing the toughness of the composite [24]. The work of fracture term, $W_F$, accounts for the mechanisms used in toughening ceramics and ceramic-ceramic composites.

In a ductile phase toughened system, in addition to the work of fracture, the work of deformation of the ductile phase adds to the energy required for crack propagation, resulting in an increase in the fracture toughness. Figure 19 shows a comparison of the fracture toughness of the Nb-18.7 a/o Si alloy, which has a continuous matrix of $Nb_3Si$, and that of the Nb-10 a/o Si alloy, which has about 47 vol. % of ductile Nb distributed in a matrix of composition Nb-18.7 a/o Si. The addition of the ductile phase to the brittle matrix increases the fracture toughness of the Nb-$Nb_3Si$ composite.

The work of deformation depends upon the flow stress, strain to failure and volume fraction of the deforming ductile phase [6-10]. Extensive debonding and ductile stretching

increases the work of deformation. The morphology and distribution of the ductile phase plays a significant role in determining the amount ductile work. If a given volume fraction of ductile phase is distributed as a large number of small particles in the matrix, the probability that a particle will intercept a crack increases. However, if the particle is very tightly bonded to the matrix, the amount of deformation the particle can undergo is limited. A very loosely bonded particle will just separate from the matrix and undergo no plastic deformation. A large particle which partly debonds from the matrix provides the best ductile phase toughening characteristics [6-10]. For a given volume fraction of the ductile phase, the optimal distribution of ductile particles would require that there be a sufficient number to increase the probability of crack interception, while maintaining a size large enough to undergo plastic deformation. The interface between the ductile phase particles and the brittle matrix should be weak enough to allow sufficient, but not complete debonding.

Effect of Nb Morphology and Grain Size

Figures 20 (a), (b), and (c) show regions of the fracture surface of a notched four-point bend specimen of the as-cast Nb-10 a/o Si alloy tested at room temperature. This specimen exhibited a fracture toughness of 11.3 MPa$\sqrt{m}$. Figures 20(a) and (b) show primary Nb particles, approximately 20 μm in size, which have debonded and undergone ductile failure. The interface between the Nb and $Nb_3Si$ phases shows that the $Nb_3Si$ phase cracked resulting in the debonding. Figure 20(c) shows another primary Nb particle, much larger in size (>100 μm) which intercepted a crack, debonded from the $Nb_3Si$ phase, yet failed in a brittle manner. Bearing in mind that the primary Nb particles are essentially single grained, the fracture mode of the Nb phase depends not only on the extent of debonding, but also on the size and the crystallographic orientation of the particle with respect to the applied stress.

Figures 21(a) and (b) show regions of the fracture surface a specimen of the twice extruded (E2) material tested at room temperature. This specimen had a fracture toughness of 27 MPa$\sqrt{m}$. Figure 21(a) shows that the $Nb_3Si$ matrix has cracked around an Nb particle, and that the particle exhibits a dimpled ductile failure mode. The number of particles that underwent

debonding and ductile failure is greater in the E2 material than in the AC material. This is probably because multiple hot extrusion of the material has affected the primary Nb / $Nb_3Si$ interface. The extrusion of the Nb-10 a/o Si composite requires the simultaneous deformation of both the hard $Nb_3Si$ phase and the metallic Nb phase. After extrusion there is a large density of dislocations piled up against the Nb / $Nb_3Si$ interfaces [16]. This probably aided in debonding at the interface under stress.

Figure 21(b) shows fracture mode that was observed in the E2 material, but not in the AC material. A polycrystalline primary Nb particle has undergone fracture. The particle is strongly bonded to the silicide matrix. Due to the constraints placed by this strong bonding, the different grains in the particle begin to fail by cleavage. This releases the constraints imposed by the matrix. The grains are now able to undergo plastic deformation and ductile failure, which manifests itself as deep ductile ridges along the grain boundaries. These ductile steps are regions where considerable plastic deformation has occurred.

At room temperature, only about 15% of the primary Nb particles in the as-cast material (AC) undergo debonding and ductile failure, while the majority of particle cleave. In the twice extruded material (E2) the volume fraction of the primary Nb particles that have undergone ductile failure increases to approximately 35%.

Effect of Matrix $Nb_3Si$ and Secondary Nb phases

Figure 21(c) shows the fractured $Nb_3Si$ phase of the E2 material. The fracture surface is not flat, and appears facetted, with the size of the facets equal to the grain size of the $Nb_3Si$ phase. Secondary Nb particles, seen distributed along the grain boundaries of the $Nb_3Si$ phase, have not debonded from the matrix. However, because of their small size they all have failed in a ductile manner, pulling to "knife edges" upon fracture. A similar fracture behavior of the $Nb_3Si$ and secondary Nb phases was observed in the E1 material also. In the as-cast material, the secondary Nb particles undergo ductile failure, as in the E1 and E2 materials, but since the $Nb_3Si$ grain size is considerably larger, the fracture surface was observed to be flat and un-facetted. This indicates that during the fracture of both E1 and E2 materials, while a crack is propagating through the silicide phase, the crack tip changes direction as it moves from one grain

to the next, resulting in an increase in the fracture surface area. This increase in surface area probably contributed to some increase in the fracture toughness, through the term $W_S$ in Eq. 9.

Effect of Temperature

At low temperatures, there is little plastic deformation of the ductile phase, i.e., $\varepsilon$ in Eq. 9 is small. The strain energy release rate $\zeta_R$ and the fracture toughness $K_Q$ are affected most by $W_F$. Significant changes in the bend strength are therefore observed for small changes in $K_Q$. As temperature is increased, the strength of the composite decreases, but more ductile deformation is observed in the Nb particles. The plastic deformation energy term, therefore, plays a more significant role in the fracture toughness of the material, and, even small changes in the strength result in significant changes in the fracture toughness.

A small area of the fracture surface of the re-extruded material tested at 1000°C is shown in Figure 22. It is clear that almost all the primary Nb phase have undergone a ductile fracture. The cleavage fracture of primary Nb particles observed earlier in the as-cast and re-extruded condition at room temperature is not observed here. Extensive micro-cracking is observed in the $Nb_3Si$ matrix, indicating that the matrix is still behaving in a brittle manner, as shown in Figure 23. The primary as well as the secondary Nb particles have undergone high degree of plastic deformation, being stretched to a wedge or chisel shape. So, the contribution to the fracture toughness from the plastic work is very significant, at high temperatures for the re-extruded material.

**Ductile Phase Toughening in Nb-10 a/o Si in-situ composite**

Toughening of this composite is clearly not achieved by one energy absorption mechanism. Rather, several mechanisms including crack bridging, crack deflection, crack blunting, micro-crack toughening, etc., contribute to the toughness of this composite. However, quantifying the contribution of each individual mechanism is difficult to assess. Assuming ductile phase crack bridging is the major contributor to the improvements in fracture toughness of the alloy at room temperature, then the fracture toughness of the composite $K_C$ can be expressed as

[25,26]:

$$K_C = \left[ \frac{E_C f_m K_m^2}{E_m} + \chi f_d E_C \sigma_d a_d \right]^{1/2} \quad (10)$$

where $K_m$ is the fracture toughness of the matrix; $E_C$ is the elastic modulus of the Nb+$Nb_3Si$ composite; $E_m$ is the elastic modulus of the $Nb_3Si$ matrix phase; $f_m$ and $f_d$ are the volume fractions of the matrix and ductile phases, respectively; $\sigma_d$ and $a_d$ are the yield strength and the radius of the ductile phase; and $\chi$ is the normalized work of rupture of the ductile particle undergoing deformation and fracture while being constrained by the elastic matrix.

The parameter $\chi$ can be considered to be a measure of ductile phase toughening. Higher values of $\chi$ mean that the ductile phase has caused an increase in fracture toughness of the composite by crack bridging. The parameter is related to the area under the load extension curve for a ductile phase deforming to failure. Therefore, $\chi$ can be expressed as:

$$\chi = \frac{K_C^2 - \frac{E_C}{E_m} f_m K_m^2}{f_d E_C \sigma_d a_d} \quad (11)$$

In Nb-10 a/o Si in-situ composite system, the fracture toughness is observed to increase significantly, from about 11 to 27 MPa$\sqrt{m}$, with thermomechanical processing. Based on these measurements and on microstructural observations, the work of rupture parameter $\chi$ was calculated for the AC, E1 and E2 materials tested at room temperature, as shown in the appendix.

As shown in the previous section, though the Nb particles are supposed to be ductile, many Nb particles undergo cleavage fracture. The number of primary Nb particles that were brittle decreases in order from the AC to the E1 and the E2 conditions. The fraction of primary Nb particles that were ductile was approximately 0.15 for the AC, 0.25 for the E1, and 0.35 for the E2 materials. Clearly, the decrease in primary Nb particle size with extrusions is associated with an increase in the number of particles that failed in a ductile manner. Also, the number of Nb particles that were pulled out from the matrix in E2 condition is larger that in as-cast material. This may be due to a higher degree of constraint imposed by the matrix in AC condition than

in E2 condition. The size of secondary Nb particles formed during the eutectic transformation does not undergo significant changes due to TMP, and is assumed to be 1$\mu$m. All of the secondary Nb particles, representing about 10% of the volume of the alloy, behave in a ductile manner in all three conditions. The total volume fraction of the ductile phase in the composite, $f_d$, is the sum of the volume fraction of the secondary Nb and the volume fraction of the ductile primary Nb, and the radius of the ductile phase, $a_d$, is the weighted average of the radii of the ductile primary Nb particles and the secondary Nb particles. The normalized work of rupture parameter, $\chi$, calculated for each of the thermomechanical condition is shown in Table IV.

The value of $\chi$ is system specific and strongly depends on the geometric constraint and the interface between the ductile phase and the brittle matrix. Though the volume fraction of Nb phase is about 0.7 in Nb-10 a/o Si alloy, the low $\chi$ value of 1.11 for as-cast condition reveals that metallic Nb phase is providing little toughening of the alloy. After thermomechanical processing, larger volume fractions of the primary Nb phase become ductile. Correspondingly, the values of $\chi$ and $K_Q$ increase. Many composites which in ductile phase toughening is effective have $\chi$ values in excess of 4 [27]. As can be seen from Table VI, work of rupture parameter for the Nb-10 a/o Si system exceeds this value only after two hot extrusions.

The change the normalized work of rupture parameter $\chi$ can be correlated to the accompanying microstructural features in the following manner. In the as-cast condition, the primary Nb particles are single grains. Recrystallization that occurs during successive extrusion steps changes the single grain Nb particles to a fine polygrain structure, with each step reducing both grain size and the particle intercept size length perpendicular to the extrusion direction. Figure 24 shows the effect of TMP on the work of rupture parameter $\chi$ and the number of grains N per primary Nb particle on a plane perpendicular to the extrusion direction, where N is defined as:

$$N = \left(\frac{D_{Nb}}{d_{Nb}}\right)^2 \qquad (12)$$

where, $D_{Nb}$ is the mean intercept size of primary Nb particles perpendicular to the extrusion direction, and $d_{Nb}$ is the grain size of primary Nb phase.

These results clearly demonstrate that the mechanical behavior of a refractory metal based composite, such as Nb-10 a/o Si alloy, can be improved considerably by tailoring the microstructure through TMP. This desired microstructure consists of a fine grain silicide matrix reinforced with polygrain Nb particles which are elongated, oriented and aligned in a direction transverse to crack propagation. The powder processing route can achieve a fine grain structure which would exhibit high strength. But, significant improvements in fracture toughness would probably not be possible because factors such as the elongation, alignment, and orientation of the ductile reinforcement phase are critical and provide additional energy absorption mechanisms such as pull-out, interface sliding, and crack bridging.

The Directional Solidification (DS) process can produce a composite with reinforcing phase particles of specific size, spacing, and orientation. However, in the DS material both the matrix and the ductile particles have single grain structures, which are prone to cleavage. Therefore, thermomechanical processing by hot extrusion of a DS material will result in a fine grained oriented ductile phase toughened in-situ composite with optimum mechanical properties.

## SUMMARY AND CONCLUSIONS

1. Nb-10 a/o Si is an in-situ composite consisting of a brittle $Nb_3Si$ matrix and a ductile Nb phase. Tailoring of the microstructure by multiple hot extrusion results the refinement, alignment and orientation of both Nb and $Nb_3Si$ phases in the extrusion direction.

2. The fracture toughness and bend strength of the alloy in the as-cast (AC), once-extruded (E1) and twice-extruded (E2) conditions were evaluated at temperatures in the range of 25° to 1200°C. In the E2 condition, the room temperature fracture toughness of the alloy was about 27 MPa$\sqrt{m}$, and the strength of the alloy was in excess of 625 MPa at 1000°C, which compares well with nickel base superalloys, such as PWA 1480.

3. The fracture toughness of Nb-10 a/o Si alloy in the stable $Nb_5Si_3$+Nb condition showed a similar changes with processing as the meta-stable $Nb_3Si$+Nb composite. However at temperatures below 1200°C, $Nb_3Si$+Nb composite showed consistently better properties than the $Nb_5Si_3$+Nb.

4. Fractography of the Nb-10 a/o Si alloy in the as-cast condition revealed that the fracture surface was flat and most of the primary Nb particles had failed by cleavage. Only about 15% of all the primary Nb particles failed in a ductile manner. In the re-extruded condition the fracture surface is not flat, and about 35% of the primary Nb particles underwent ductile fracture. An additional mode of fracture involving the formation of ductile ridges in the primary Nb particles was observed. The fracture mode of the silicide matrix in the re-extruded material appeared to be the same as that of the as-cast material, essentially exhibiting a flat cleavage fracture. More micro-cracks were observed in the silicide matrix of the re-extruded material. The secondary Nb particles had experienced a high degree of ductile phase toughening stretching to a wedge or chisel shape.

5. The degree of ductile phase toughening resulting from TMP of the Nb-10 a/o Si alloy, was characterized by the normalized work of rupture parameter $\chi$. The value of $\chi$ was found to increase from 1.11 for the as-cast material to 3.13 for extruded (E1) material and

then to 8.87 for the re-extruded (E2) material. The normalized work of rupture ($\chi$) parameter was related to the number of grains per primary Nb particle on a plane perpendicular to the extrusion direction.

6. The optimum microstructure of a ductile phase toughened in-situ composite is elongated polycrystalline particles of the ductile phase distributed in a fine grained matrix. Multiple hot extrusion of a cast in-situ composite can tailor this microstructure. Another recommended processing sequence is the directionally solidify (DS) the two phase composite to initially create ductile phase particles aligned in a suitable direction, and then thermomechanically process the DS cast structure, by a process such as hot extrusion, to produce the fine grained, oriented microstructure.

## REFERENCES


1. A.K. Vasudevan and J.J. Petrovic, Proceedings of the First High Temperature Structural Silicides Workshop, Elsevier Sequoia, pp. 1-17, (1992).

2. P.J. Mescher and D.S. Schwartz, J. of Metals, Vol. 41, No. 11, pp. 52-56, (1989).

3. M.G. Mendiratta, J.J. Lewandowski and D.M. Dimiduk, Metall. Trans., Vol. 22A, pp. 1573-1583, (1991).

4. B.D. Flinn, M. Ruhle and A.G. Evans, Acta Metall., Vol. 37, pp. 3001-3006, (1989).

5. J.W. Newkirk and J.A. Sago, MRS Symposium Proceedings, Vol. 194, pp. 2969-2977, (1989).

6. P.A. Mataga, Acta Metall., Vol. 37, No. 12, pp. 3349-3359, (1989).

7. M.F. Ashby, F.J. Blunt and M. Bannister, Acta Metall., Vol. 37, No. 7, pp. 1847-1857, (1989).

8. A.G. Evans and R. McMeeking, Acta Metall., Vol. 34, No. 12, pp. 2435-2441, (1986).

9. A.G. Evans, "The New High Toughness Ceramics", ASM STP 907, American Society for Testing and Materials, pp. 267-291, (1989).

10. L.S. Sigl et al., Vol. 36, No. 4, pp. 945-953, (1988).

11. R.O. Ritchie, Materials Science and Engineering, Vol. A103, pp. 15-28, (1988).

12. T.B. Massalski, Binary Alloy Phase Diagrams, ASM, p 2767, (1991).

13. D. Patrizio, M.S. Thesis, Wright State University, Dayton, OH, (1991).

14. R. Srinivasan and I. Weiss, Proceedings of the Klaus Schulze Symposium on High Purity Refractory Metals and their Alloys, TMS, Warrendale, PA (to appear in 1994).

15. M. Saqib et al., PRICM-I, Proceedings of the International Pacific Rim Conference on Advanced Materials and Processing, TMS, Warrendale, Pa (1992).

16. B. Cockeram, M.S. Thesis, Wright State University, Dayton, OH, (1991).

17. M. Thirukkonda, M.S. Thesis, Wright State University, Dayton, OH, (1993).

18. ASTM Standard - E399.

19. MIL-STD-1942 (MR).

20. G.K. Bansal and W.H. Duckworth, "Fracture Surface Energy Measurements By the Notch-Beam Technique", Fracture Mechanics Applied to Brittle Materials , pp 38-46.

21 Metals Handbook Vol. 2, Properties and Selection of Nonferrous Alloys and Pure Metals, ASM, Materials Park, OH, p 778 (1979).

22. G.E. Dieter, Mechanical Metallurgy , 3rd ed., McGraw-Hill, (1986).

23. G. Petzow, R. Telle and R. Danzer, Materials Characterization , Vol. 26, pp. 289-302, (1991).

24. T.L. Anderson, Fracture Mechanics : Fundamentals and Applications , CRC Press, pp. 394-408, (1991).

25. R.N. Nekkanti and D.M. Dimiduk, MRS Proceedings , Vol. 194, pp. 175-182, (1990).

26. M.G. Mendiratta and D.M. Dimiduk, Metall. Trans., Vol. 24A, pp. 501-504, (1993).

27. K.S. Ravichandran, Scripta Metall., Vol.. 26, pp 1389-1393, (1992).

**Table I: Evolution of Microstructural Parameters during Thermomechanical Processing of Nb-10 a/o Si alloy**

| Microstructural Parameter | As-Cast Condition (AC) | Once-Extruded Condition (E1) | Twice-Extruded Condition (E2) |
|---|---|---|---|
| Mean Intercept length of Primary Nb, $D_{Nb}$ | 20 $\mu$m * | 16 $\mu$m # | 11 $\mu$m # |
| Grain size of Primary Nb, $d_{Nb}$ | 20 $\mu$m * | 11 $\mu$m | 6 $\mu$m |
| Aspect ratio of Primary Nb, $\phi_{Nb}$ | 1 | 4 | 14 |
| Interparticle spacing Primary Nb, $\lambda_{Nb}$ | 14 $\mu$m * | 11 $\mu$m # | 6 $\mu$m # |
| Grain size of $Nb_3Si$ phase, $d_{Nb_3Si}$ | 18 $\mu$m * | 5 $\mu$m | 2 $\mu$m |

* Measured for all orientations
\# Measured perpendicular to extrusion direction

**Table II : Bending Strength of Nb-10 Si a/o Alloy**

| Thermomechanical Condition | Test Temp.( °C) | $\sigma_y$ (MPa) | $\sigma_f$ (MPa) |
|---|---|---|---|
| As Cast - Nb+$Nb_3Si$ | 25 | x | 334 |
| (AC ) | 1000 | 356 | 484 |
| | 1200 | 289 | 435 |
| Extruded - Nb+$Nb_3Si$ | 25 | x | 795 |
| (E1) | 1000 | 445 | 668 |
| | 1200 | 365 | + |
| Re-extruded - Nb+$Nb_3Si$ | 25 | x | 1344 |
| (E2) | 560 | 1070 | 1438 |
| | 800 | 882 | + |
| | 1000 | 638 | + |
| | 1200 | 402 | + |
| Extruded - Nb+$Nb_5Si_3$ | 25 | 512 | 700 |
| (E1+HT) | 1000 | 389 | + |
| | 1200 | 321 | + |
| Re-extruded - Nb+$Nb_5Si_3$ | 25 | 806 | 1188 |
| (E2+HT) | 600 | 904 | + |
| | 1000 | 529 | + |
| | 1200 | 462 | + |

Note:

+ indicates specimens that did not fail, but bottomed out.
x indicates specimens that failed in a brittle manner.

**Table III : Fracture toughness of Nb-10 a/o Si alloy**

| Thermo-mechanical Condition | Temperature (°C) | $K_Q$ MPa$\sqrt{m}$ |
|---|---|---|
| As-Cast - Nb+$Nb_3Si$ (AC) | 25 | 11 to 15 |
| | 1000 | 18.8 |
| | 1200 | 17.5 |
| Extruded - Nb+$Nb_3Si$ (E1) | 25 | 21.4 |
| | 600 | 32.8 |
| | 1000 | 29.4 |
| | 1200 | 27.7 |
| Extruded - Nb+$Nb_5Si_3$ (E1+HT) | 25 | 21.0 |
| | 1000 | 22.0 |
| | 1200 | 19.6 |
| Re-extruded - Nb+$Nb_3Si$ (E2) | 25 | 27.0 |
| | 600 | 35.5 |
| | 1000 | 49.1 |
| | 1200 | 47.4 |
| Re-extruded - Nb+$Nb_5Si_3$ (E2 + HT) | 25 | 25.1 |
| | 1000 | 28.0 |
| | 1200 | 25.3 |

**Table IV : Normalized work of rupture '$\chi$' calculation for Nb-10 a/o Si alloy**

$E_C$ = 178 GPa  $E_m$ = 400 GPa  $\sigma_d$ = 400 MPa
$K_m$ = 3 MPa$\sqrt{m}$  $f_m$ = 0.4

| Thermo-mechanical Condition | $K_C$ MPa$\sqrt{m}$ | $f_d$ | $a_d$ $\mu$m | $\chi$ |
|---|---|---|---|---|
| As-cast-Nb+$Nb_3Si$ (AC - I Gen.) | 11.3 | 0.25 | 6.4 | 1.11 |
| Extruded -Nb+$Nb_3Si$ (E1 - II Gen.) | 21.4 | 0.35 | 5.86 | 3.13 |
| Re-extruded -Nb+$Nb_3Si$ (E2 - III Gen.) | 27.0 | 0.45 | 2.56 | 8.87 |

## Appendix

### Calculation of the ductile phase toughening parameter $\chi$

The parameter $\chi$ can be considered to be a measure of toughness increase provided by ductile phase crack bridging, and can be expressed as,

$$\chi = \frac{K_C^2 - \frac{E_C}{E_m} f_m K_m^2}{f_d E_C \sigma_d \mu_d} \qquad (13)$$

The elastic modulus of the composite, $E_C$, was determined from the slope of the load versus time plot obtained from a three-point bend test on the Nb-10 a/o Si composite. The value of $E_C$ = 178 GPa compares well with the value of 195 GPa previously reported [26]. The elastic modulus of the matrix $Nb_3Si$, $E_m$, was determined from the slope of the load-time plot of a three-point bend test on the eutectic Nb-18.7 a/o Si alloy, suitably adjusted for the volume fraction of the $Nb_3Si$ phase. The value obtained for $E_m$ was about 400 GPa. Values of 3 MPa$\sqrt{m}$ and 400 MPa used for $K_m$ and $\sigma_d$ were the same as in previous studies [25]. The radius of the ductile phase particles was taken as the weighted average of the radius ductile primary Nb particles and that of the secondary Nb particles. All the secondary Nb particles, of radius 0.1 $\mu$m, representing 13 vol% of the composite, were assumed to be ductile. Only some of the primary Nb particles failed in a ductile manner. This volume fraction was estimated as 15%, 25% and 35% in the AC, E1, and E2 conditions, respectively at room temperature. The size of the primary Nb particles perpendicular to the extrusion axis was used as the radius of these particles. This radius was 10, 7.8, and 3 $\mu$m in the AC, E1 and E2 materials, respectively. Experimentally measured values of the fracture toughness of the composite, $K_C$ were used in the above equation to determine the values of $\chi$ presented in Table IV.

## List of Figures

**List of Figures** (cont)

## List of Figures (cont)

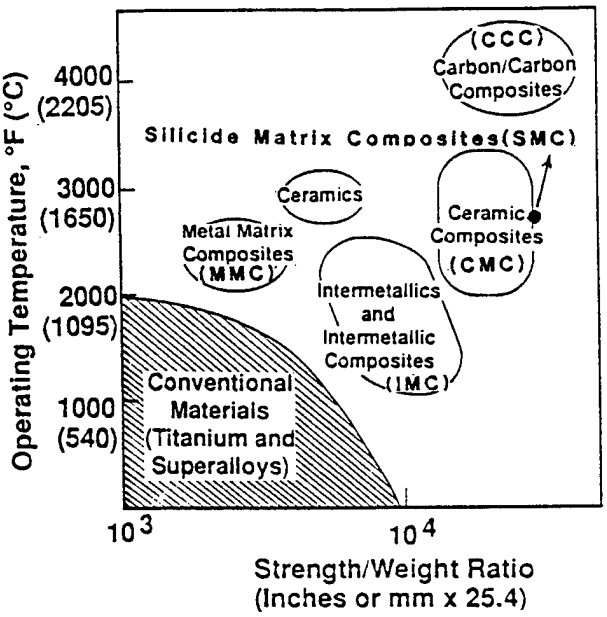


Figure 1: Operating temperatures and strength to weight ratios for various high temperature materials.

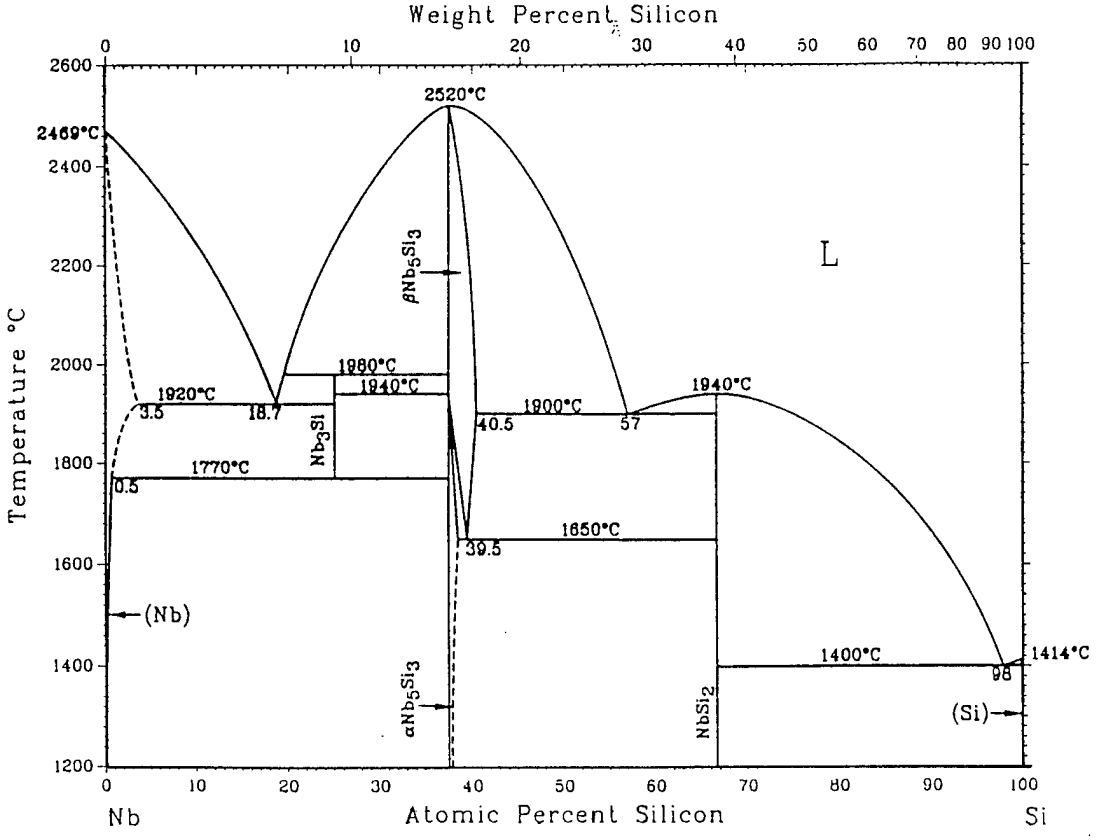


Figure 2: Phase diagram of the Nb-Si system.

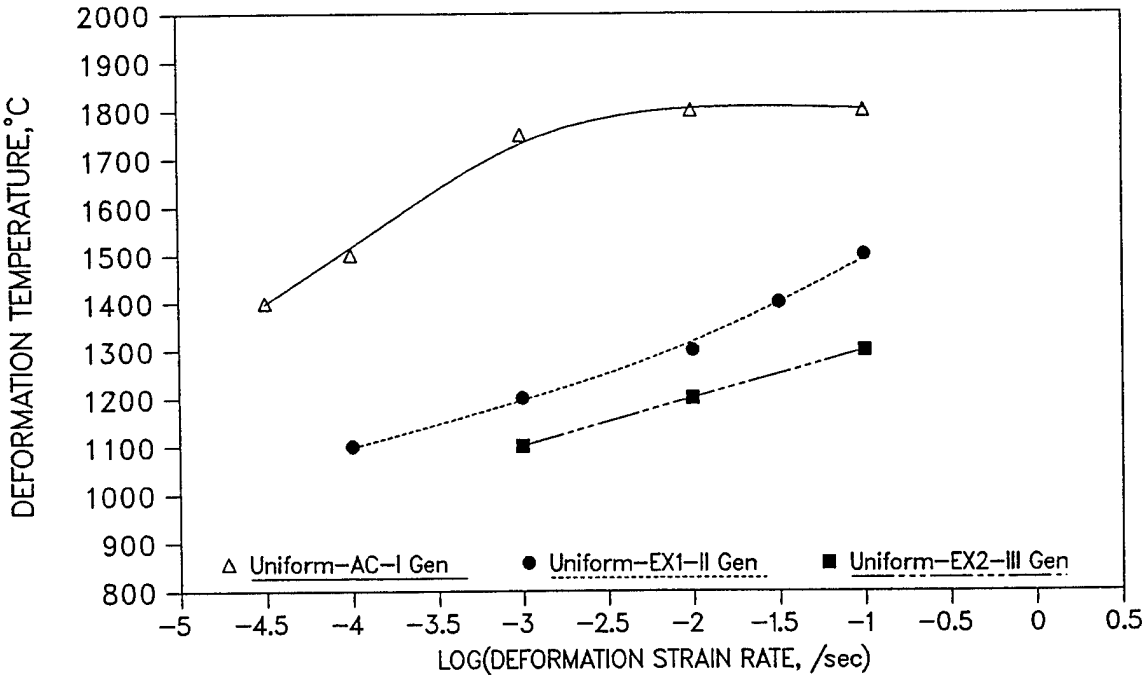


Figure 3: Processing maps for the Nb-10 a/o Si alloy in the as-cast (AC), once-extruded (E1), and twice-extruded (E2) conditions.

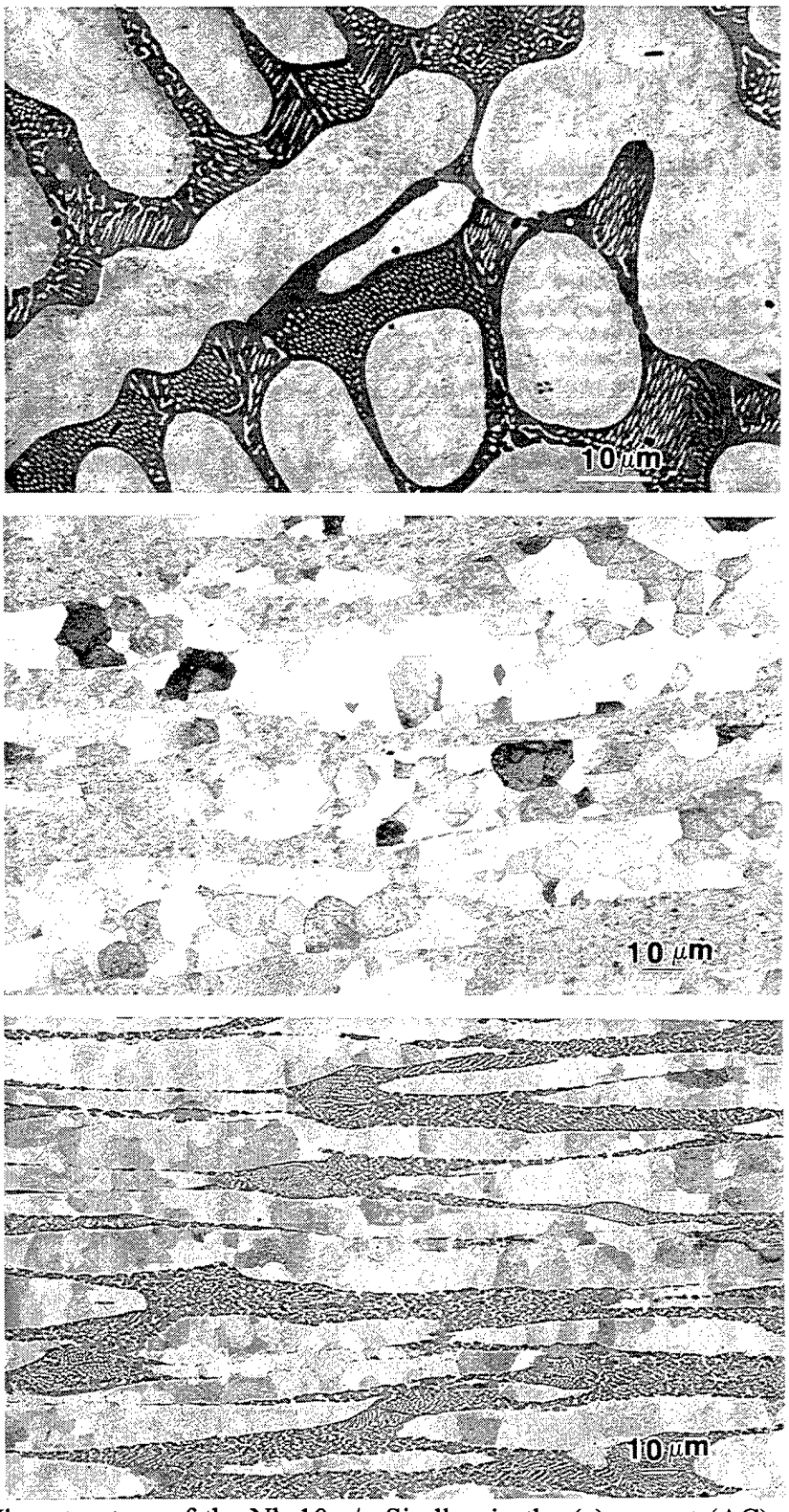


(a)

(b)

(c)

Figure 4: Microstructure of the Nb-10 a/o Si alloy in the (a) as-cast (AC), (b) once-extruded (E1), and, (c) twice-extruded (E2) conditions. The dark phase is $Nb_3Si$, and the light phase is Nb.

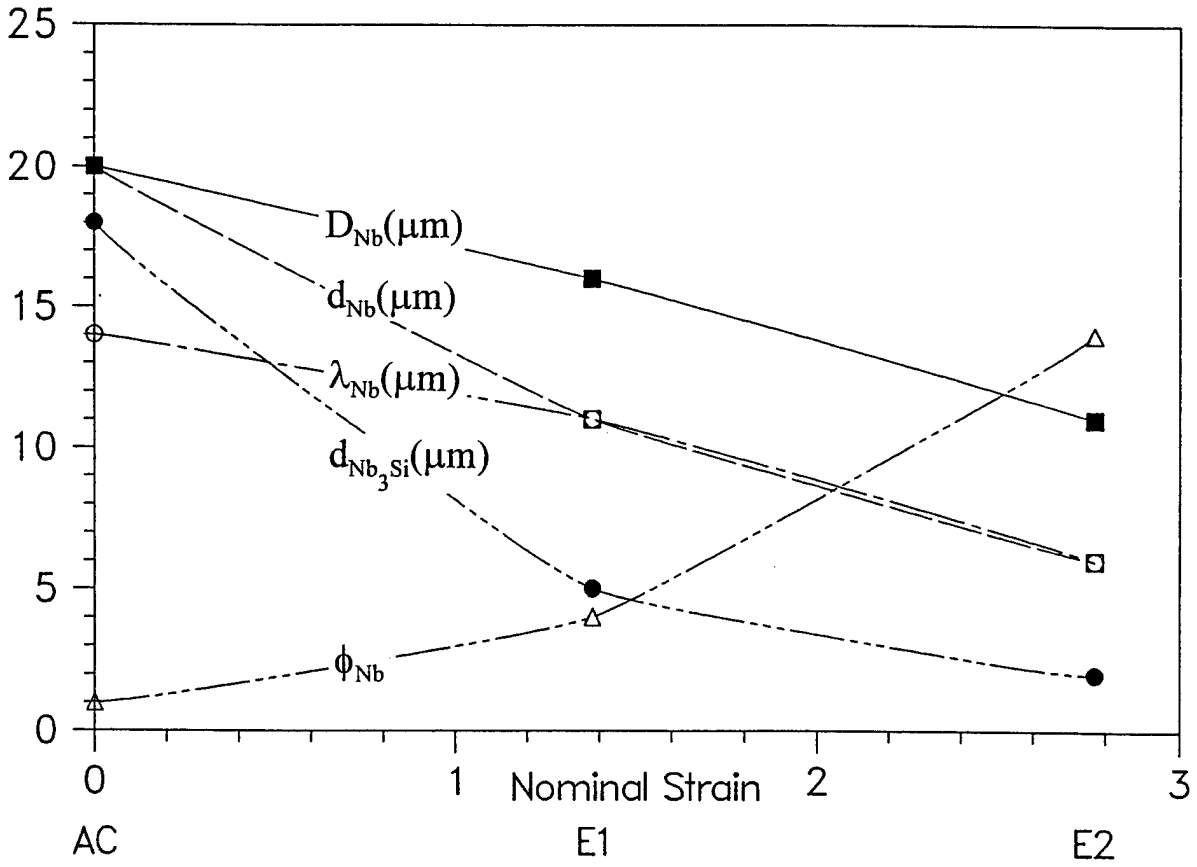


Figure 5: Effect of multiple hot extrusion on various microstructural parameters of the Nb-10 a/o Si alloy. $D_{Nb}$ = Mean intercept length the primary Nb phase perpendicular to the extrusion direction; $d_{Nb}$ = grain size in the primary Nb phase; $\lambda_{Nb}$= interparticle spacing of the primary Nb phase particles perpendicular to the extrusion direction, $d_{Nb_3Si}$ = grain size in the $Nb_3Si$ phase; $\phi_{Nb}$ = aspect ratio of the primary Nb phase particles.

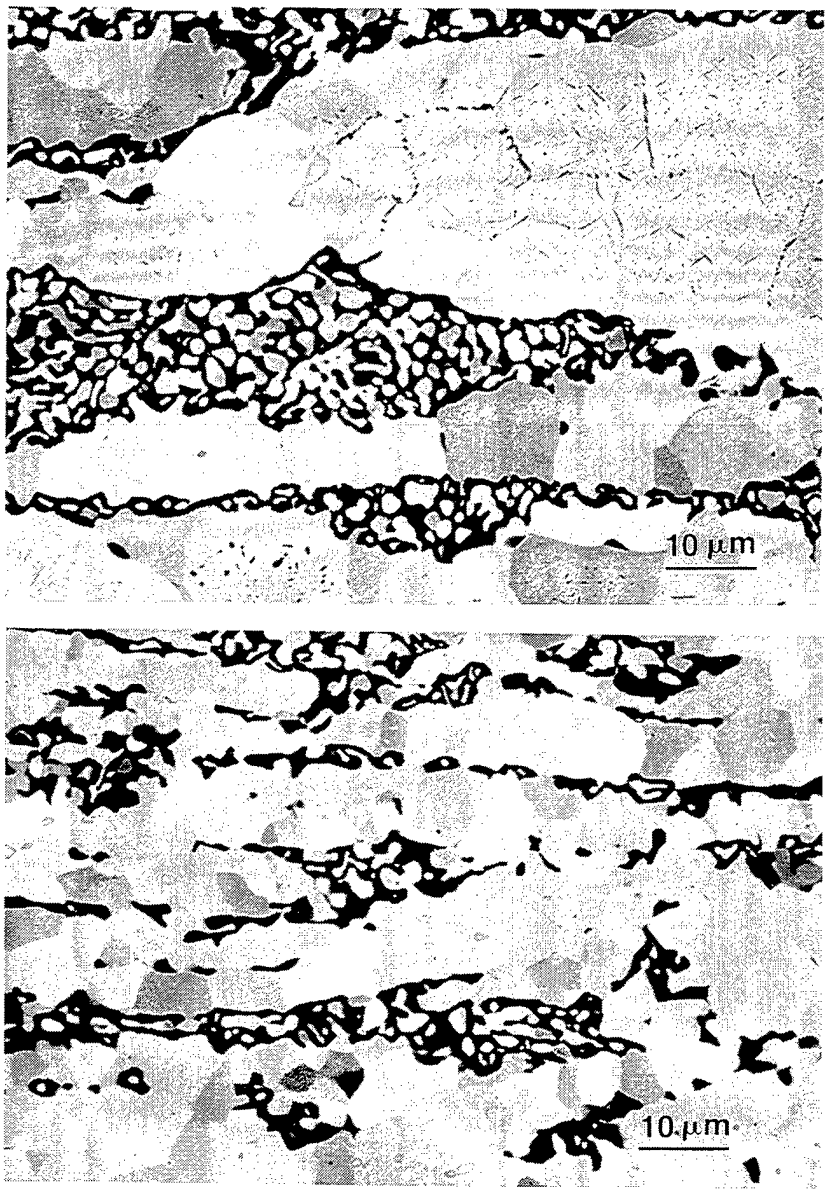


(a)

(b)

Figure 6: Microstructure of the Nb-10 a/o Si alloy in the (a) once-extruded and heat treated (E1+HT), and, (b) twice-extruded and heat treated (E2+HT) conditions. The black phase is $Nb_5Si_3$, and the light phase is Nb.

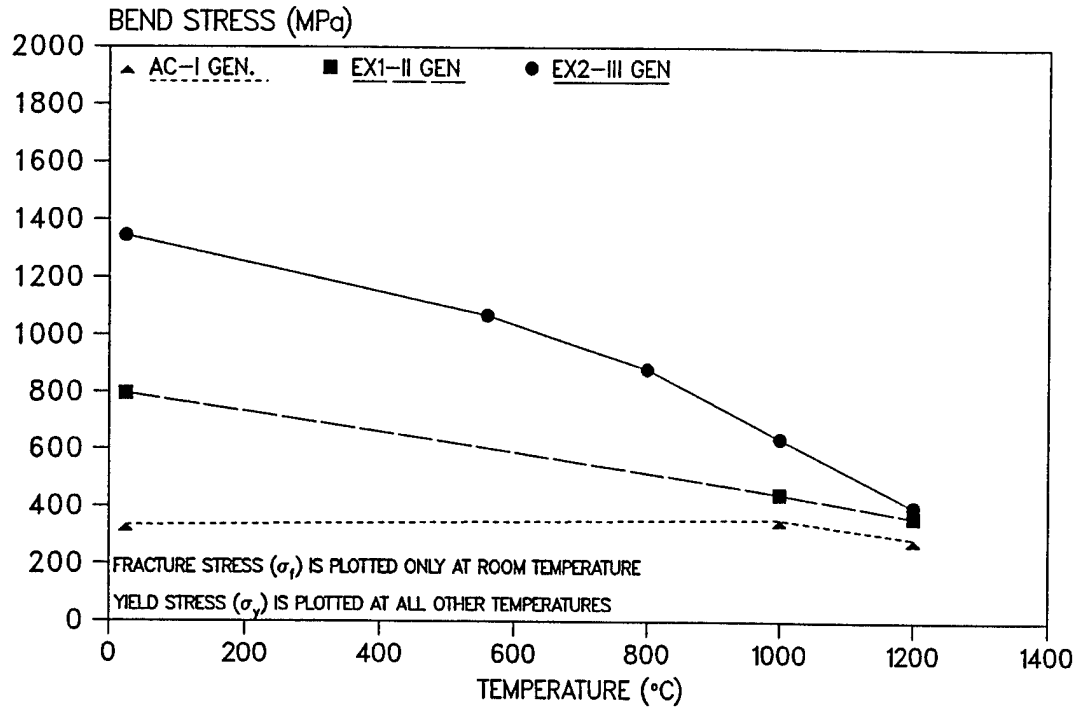


Figure 7. Variation of bend strength of the Nb-10 a/o Si alloy with temperature in the as-cast (AC), once-extruded (E1), and twice-extruded (E2) conditions.

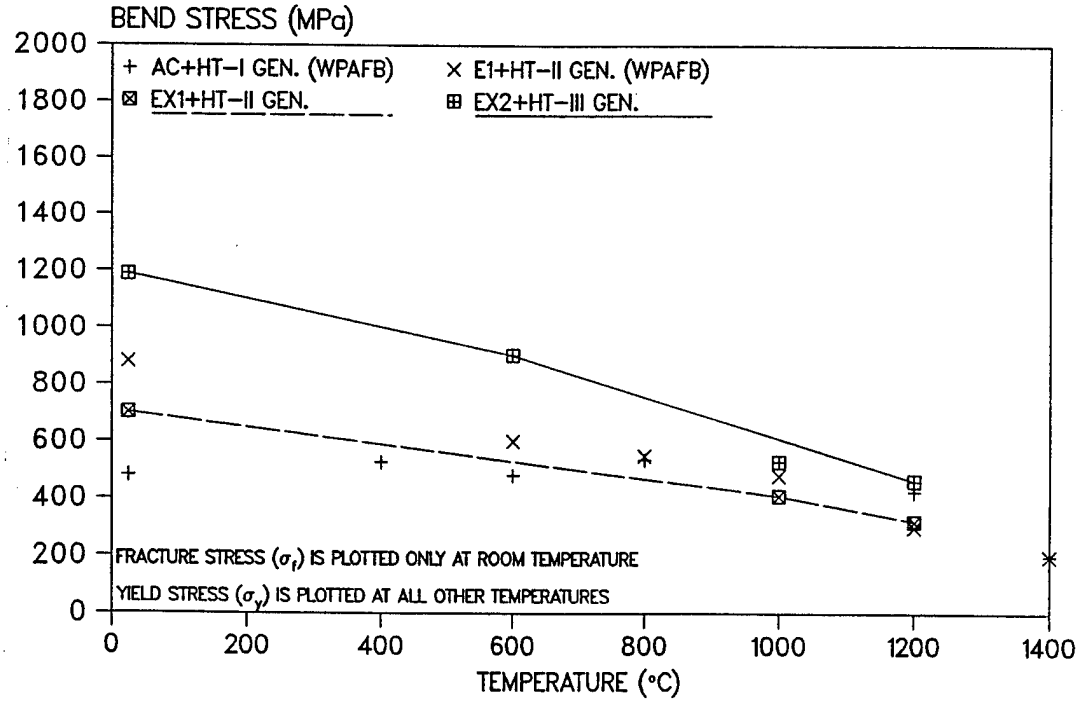


Figure 8: Variation of bend strength of the Nb-10 a/o Si alloy with temperature in the once-extruded and heat treated (E1+HT) and twice-extruded and heat treated (E2+HT) conditions.

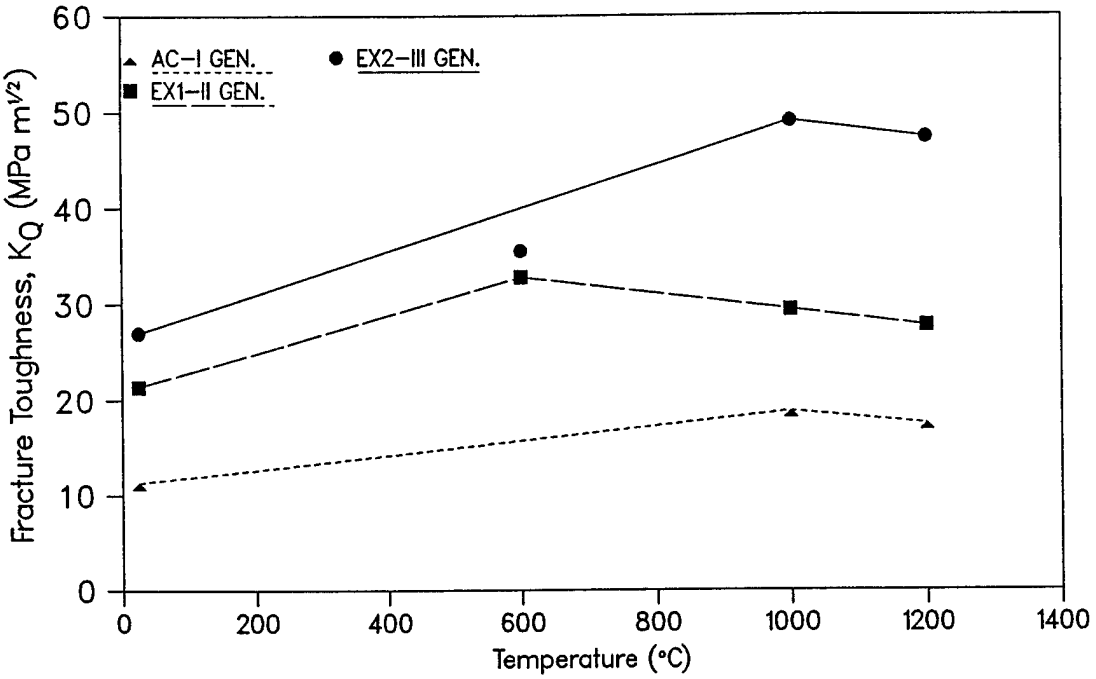


Figure 9: Variation of fracture toughness, $K_Q$, of the Nb-10 a/o Si alloy with temperature in the as-cast (AC), once-extruded (E1), and twice-extruded (E2) conditions.

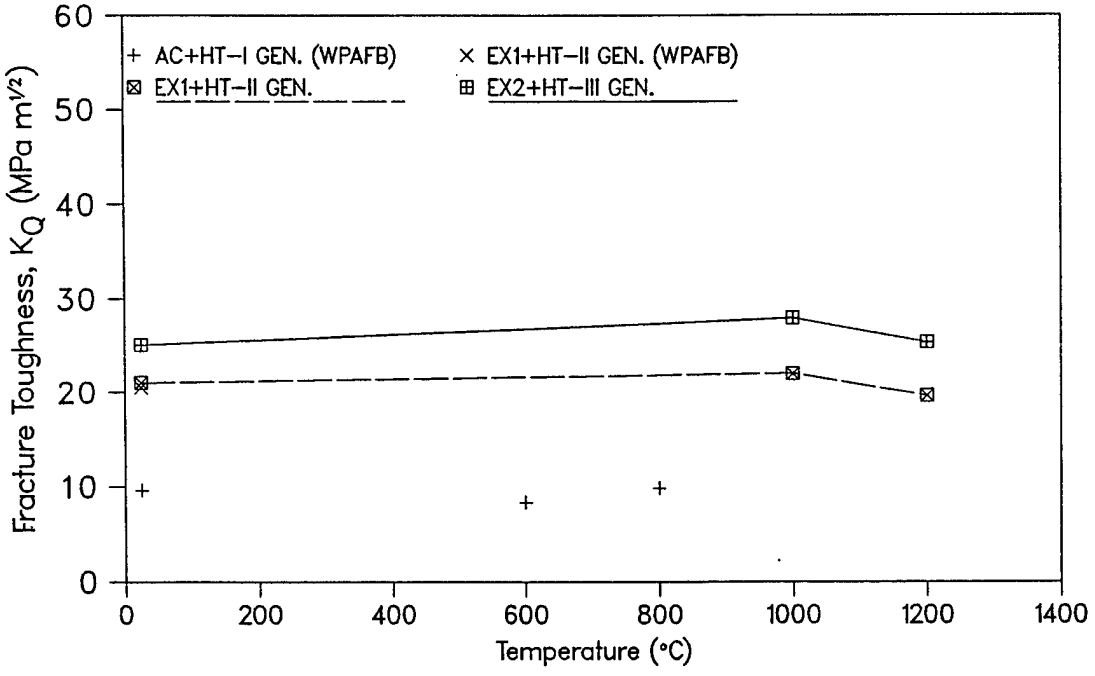


Figure 10: Variation of fracture toughness, $K_Q$, of the Nb-10 a/o Si alloy with temperature in the once-extruded and heat treated (E1+HT) and twice-extruded and heat treated (E2+HT) conditions.

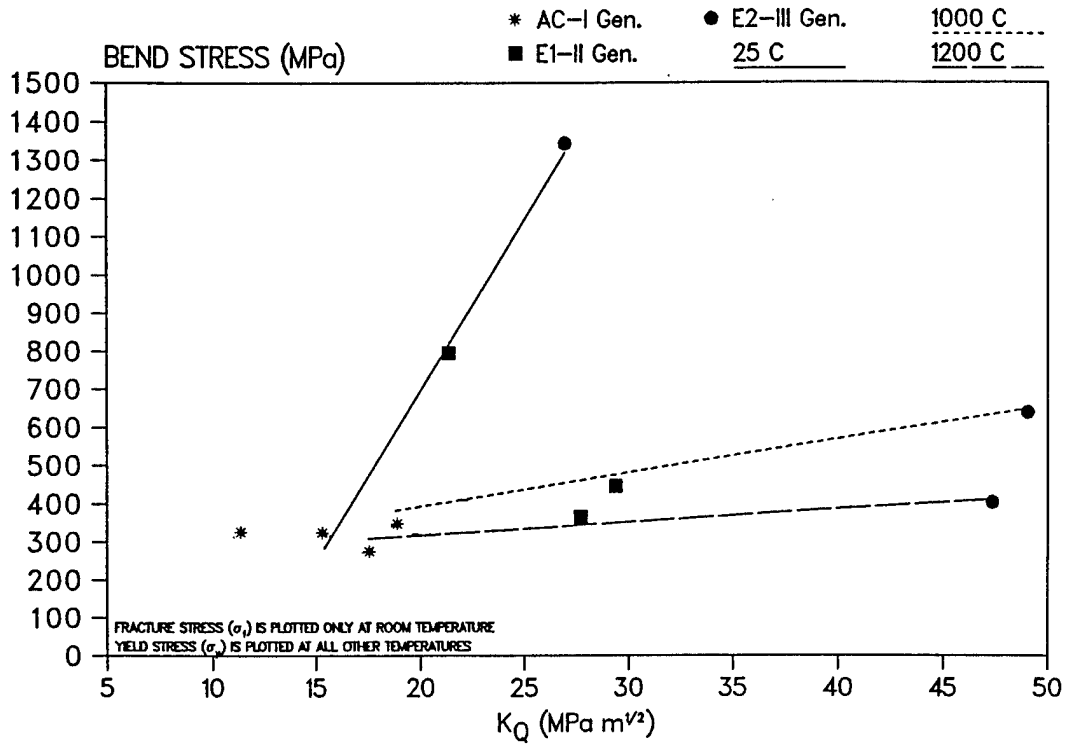


Figure 11: Effect of thermomechanical processing on the bend strength and fracture toughness of the Nb-10 a/o Si alloy at different temperatures.

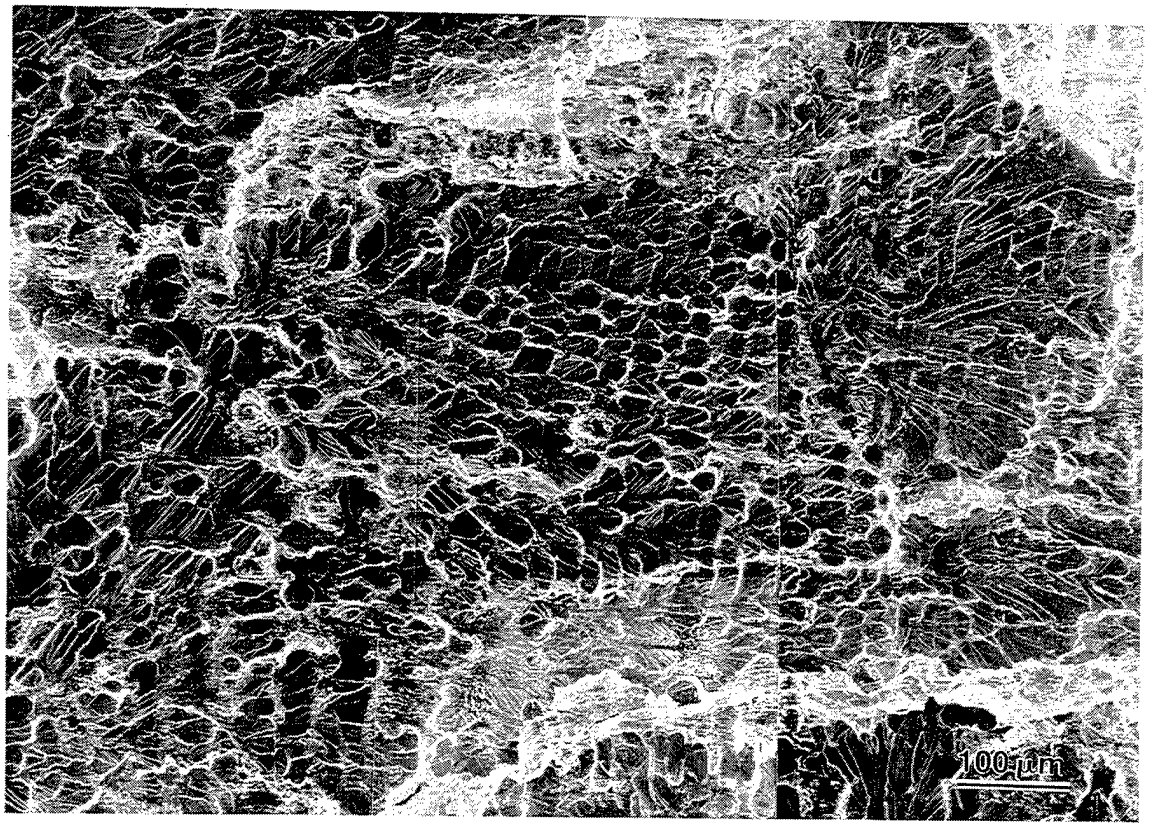


Figure 12: Fracture surface of a notched specimen of the as-cast (AC) Nb-10 a/o Si alloy tested in four-point bending at room temperature. Most primary Nb particles have undergone cleavage failure.

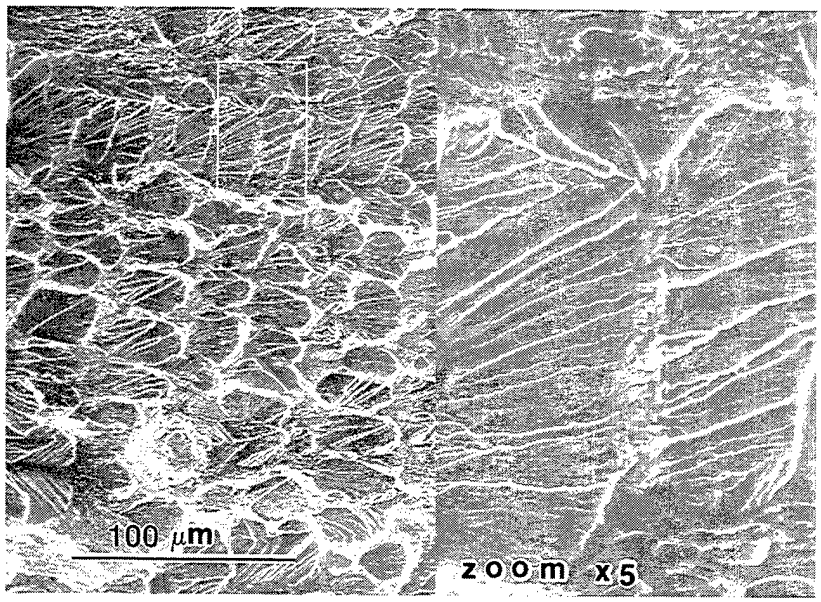


Figure 13: Micrograph showing two primary Nb particles and the $Nb_3Si$ matrix of the as-cast (AC) Nb-10 a/o Si alloy tested in four-point bending at room temperature. The Nb particles show the "river pattern" associated with cleavage fracture. The $Nb_3Si$ phase also exhibits brittle failure. The fine white speckles in the $Nb_3Si$ phase are secondary Nb particles which have undergone ductile failure.

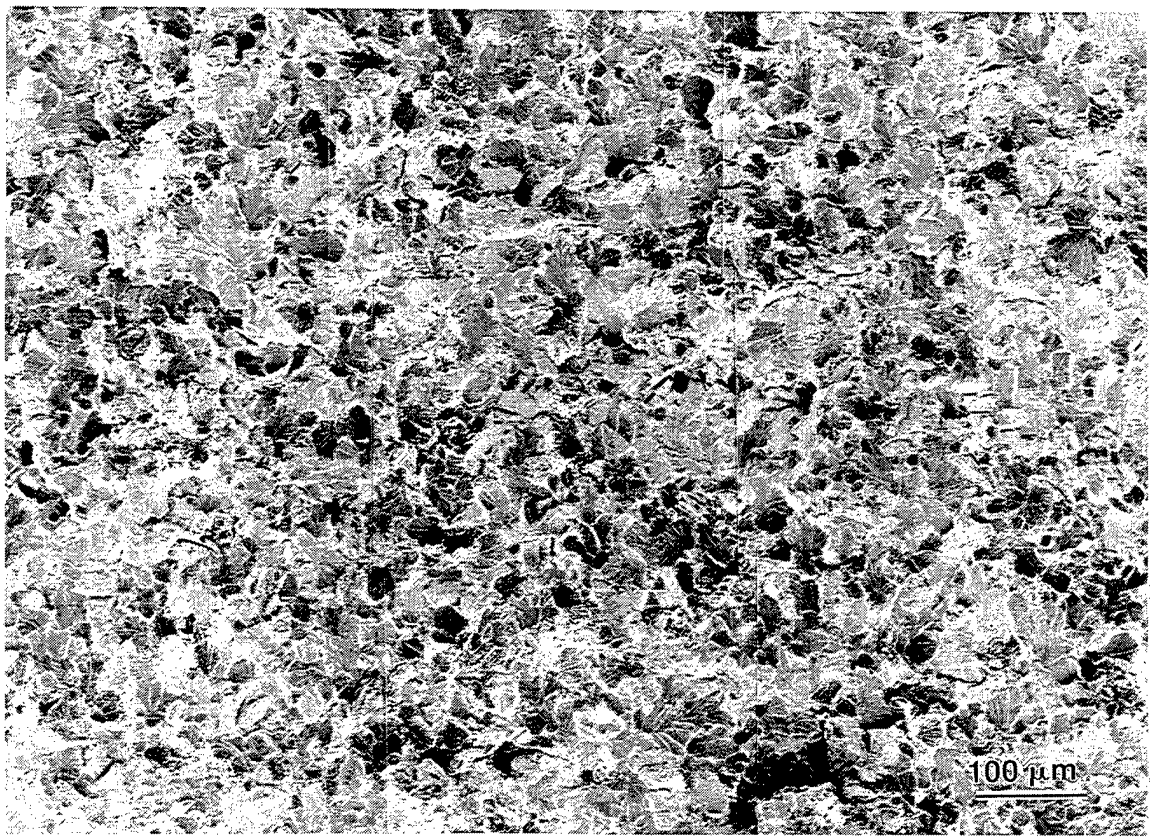


Figure 14: Fracture surface of a notched specimen of the twice-extruded (E2) Nb-10 a/o Si alloy tested in four-point bending at room temperature. Many primary Nb particles show regions of ductile deformation. The $Nb_3Si$ matrix exhibits extensive microcracking.

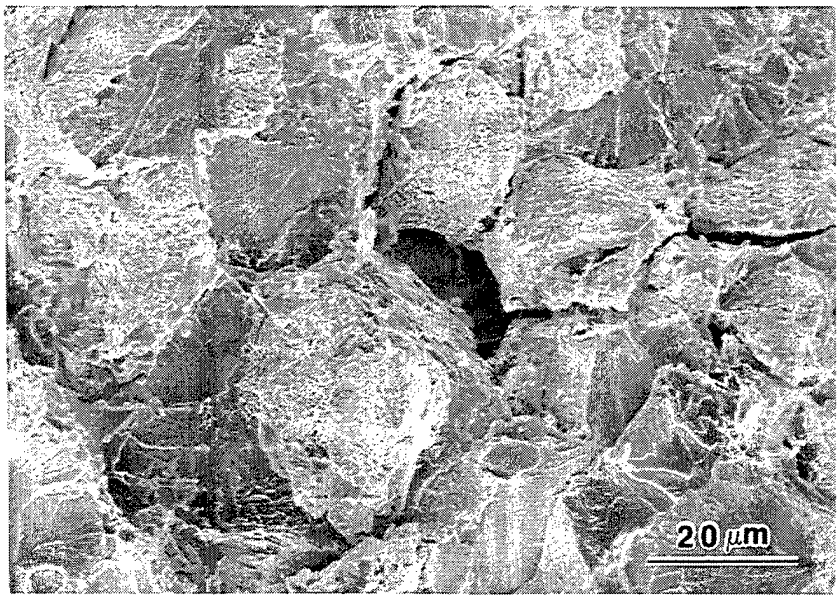


Figure 15: Micrograph showing debonding and ductile failure of a primary Nb particle on the fracture surface of a notched specimen of the twice-extruded (E2) Nb-10 a/o Si alloy tested in four-point bending at room temperature.

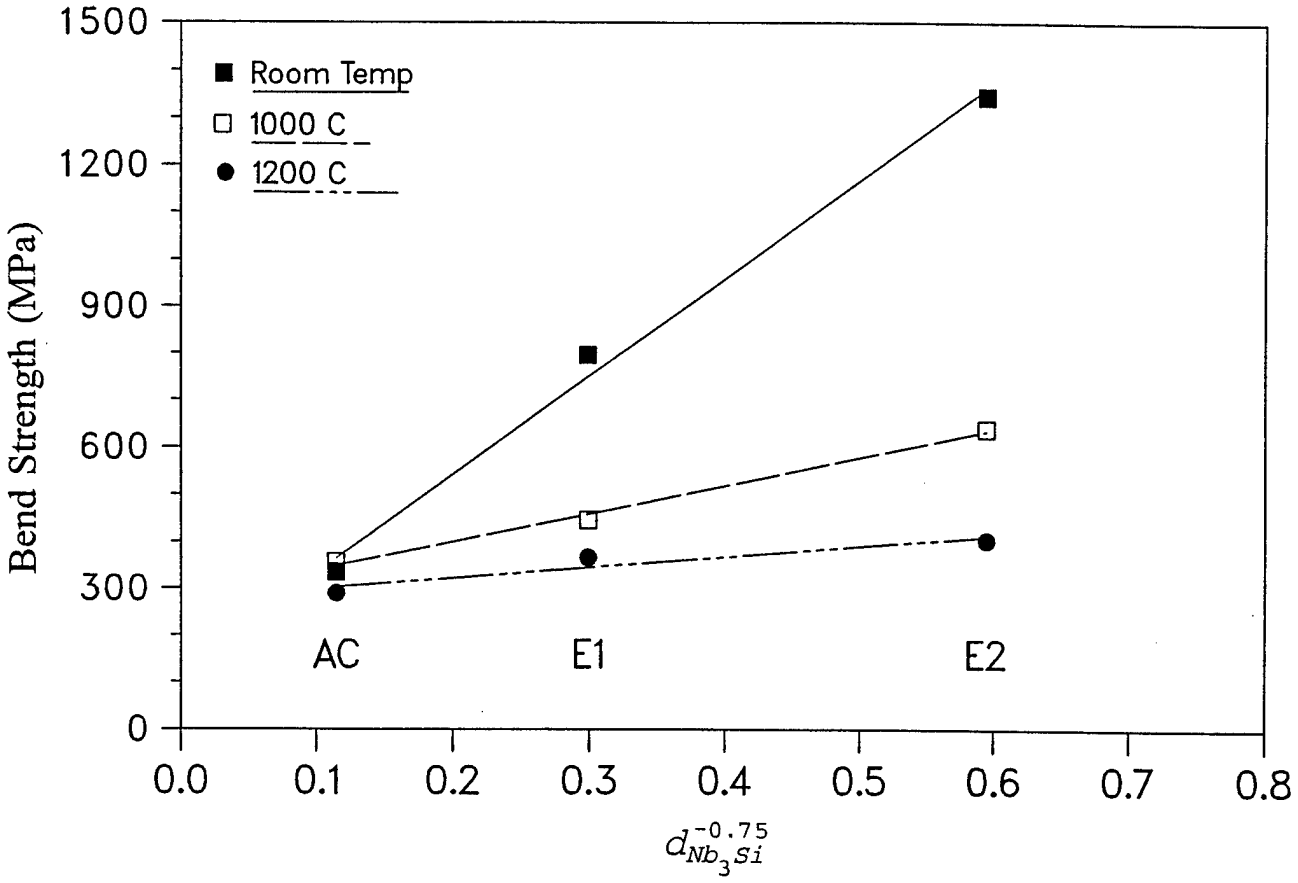


Figure 16: Variation of the bend strength of the Nb-10 a/o Si alloy with grain size in the $Nb_3Si$ phase at different temperatures.

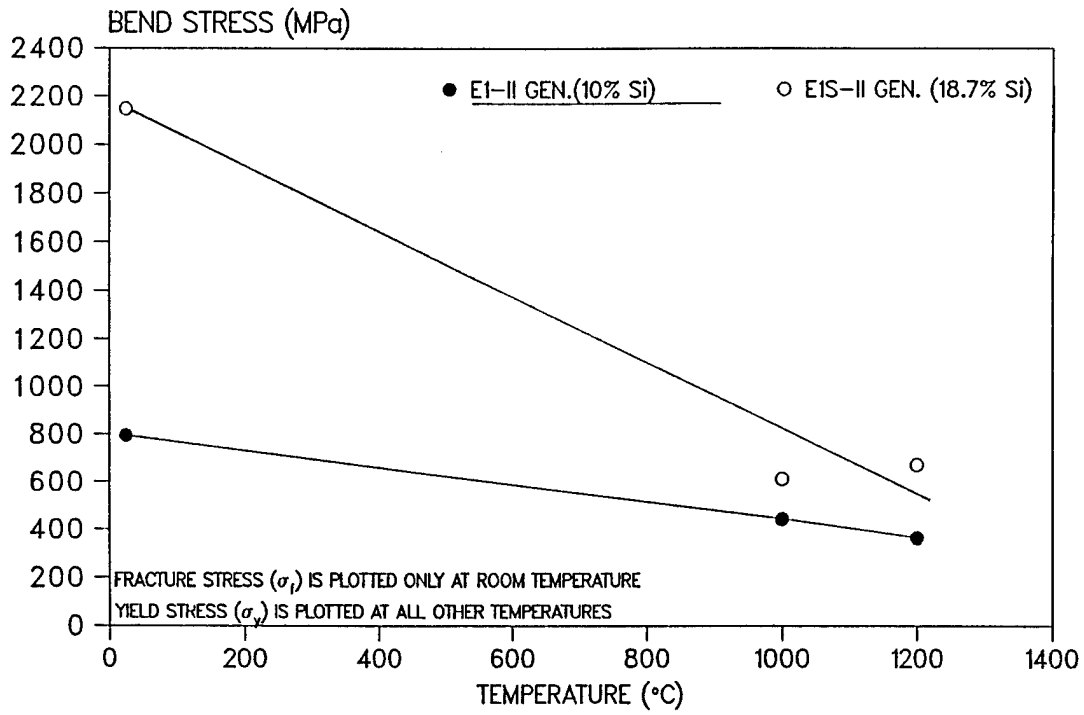


Figure 17: Comparison of the bending strength of Nb-10 a/o Si and Nb-18.7 a/o Si alloys in the E1 condition.

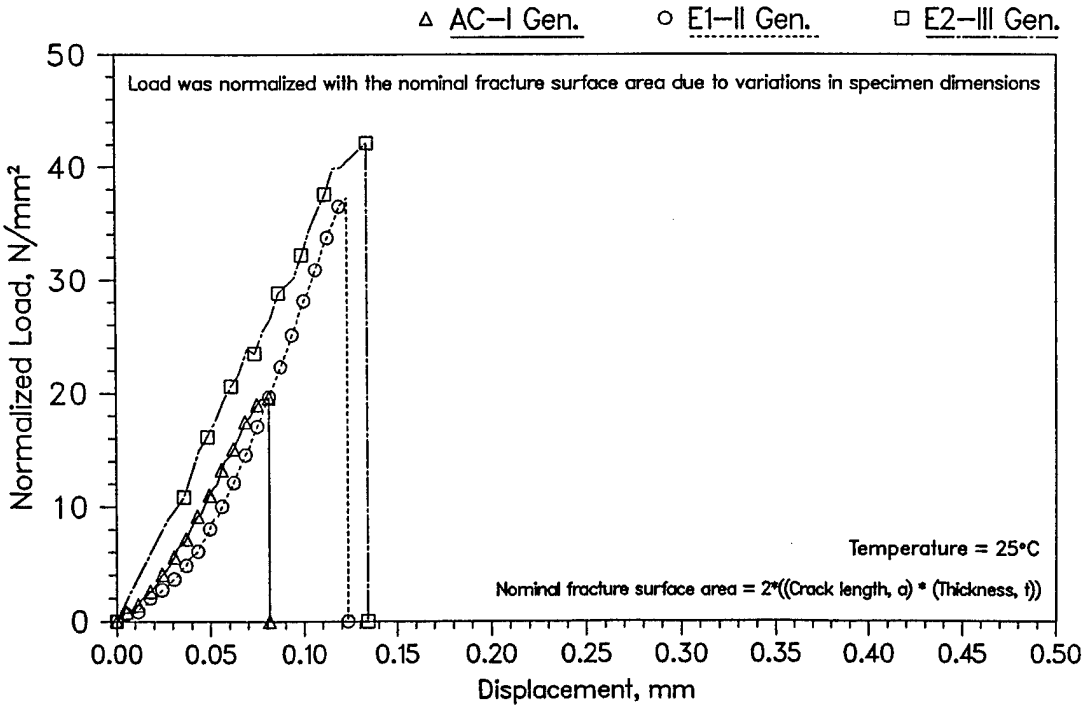


Figure 18: Normalized load versus displacement curves from tests on notched specimen of the Nb-10 a/o Si alloy in the as-cast (AC), once-extruded (E1), and twice-extruded (E2) conditions tested in four-point bending at room temperature.

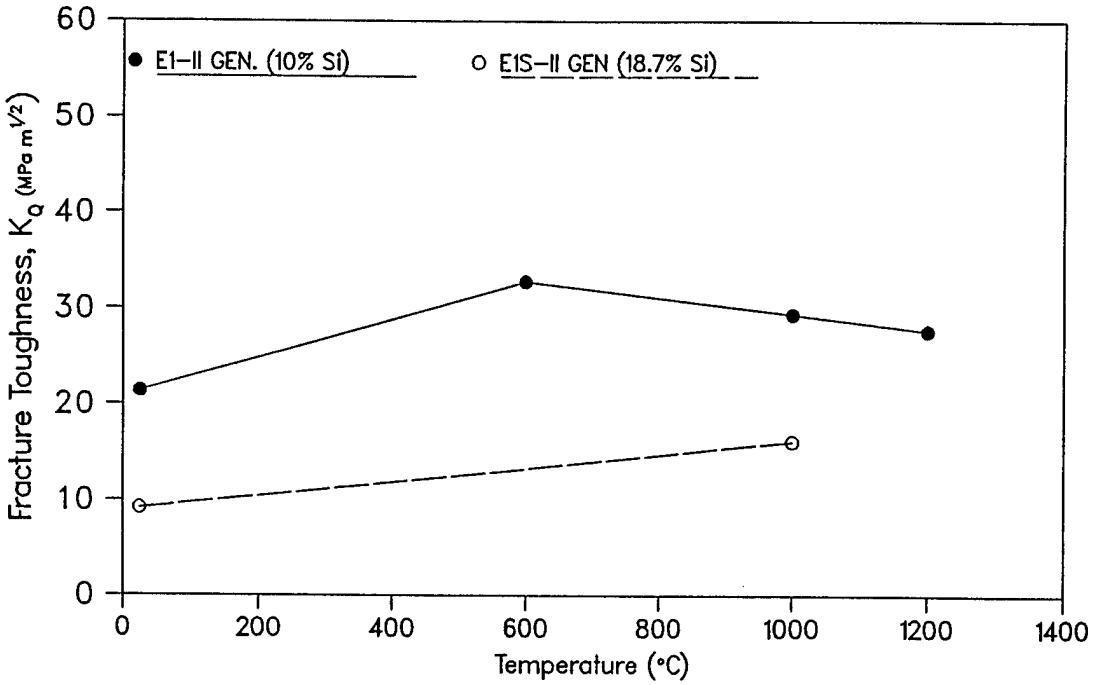


Figure 19: Comparison of the fracture toughness of Nb-10 a/o Si and Nb-18.7 a/o Si alloys in the E1 condition.

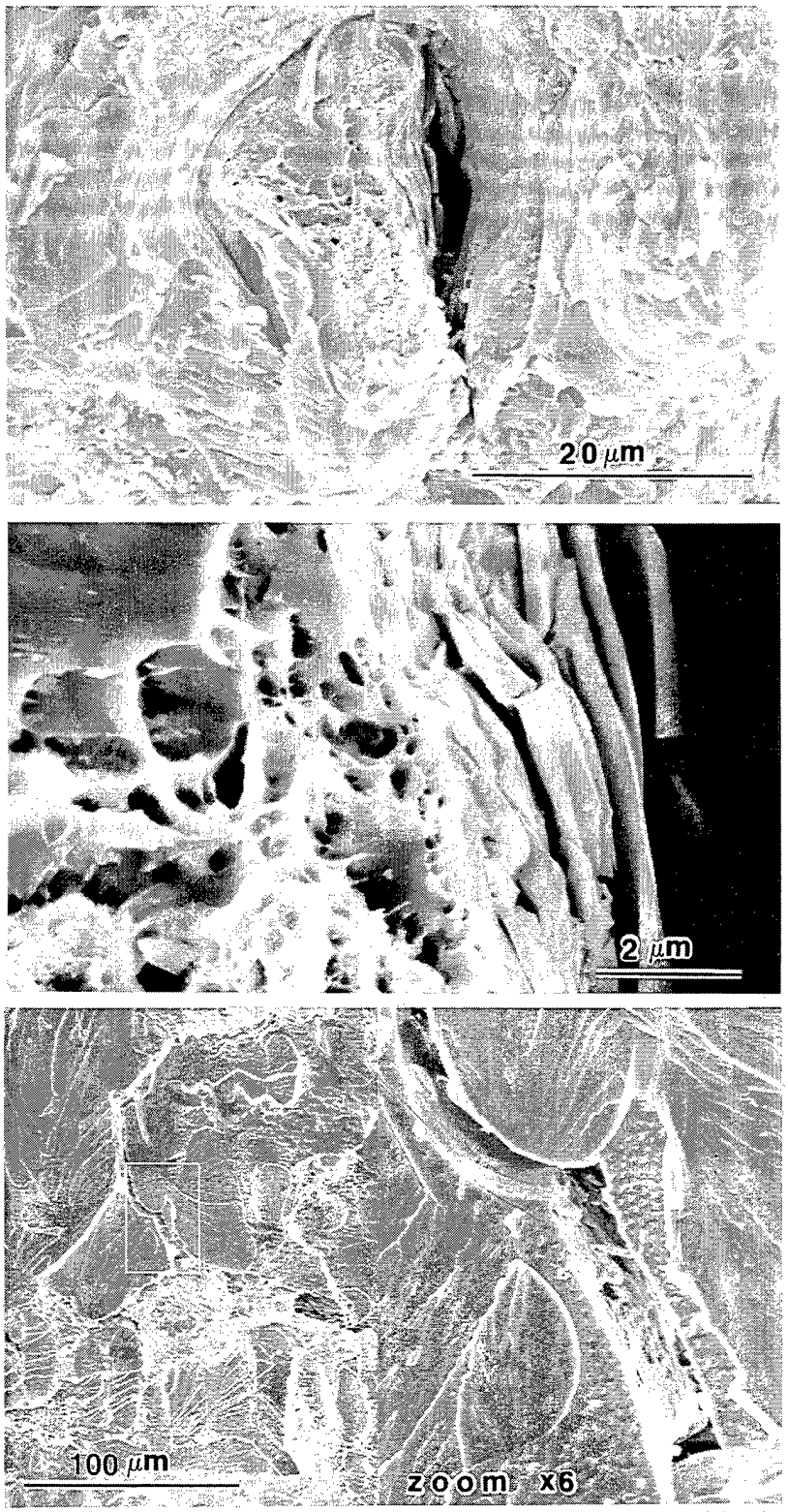


Figure 20: Fractographs of the as-cast (AC) Nb-10 a/o Si alloy tested in four-point bending at room temperature. (a) A primary Nb particle that has debonded from the $Nb_3Si$ matrix and undergone ductile failure. (b) Dimpled fracture of a primary Nb particle and brittle fracture of the $Nb_3Si$ matrix at the interface. (c) Brittle fracture of a primary Nb particle in spite of debonding from the matrix.

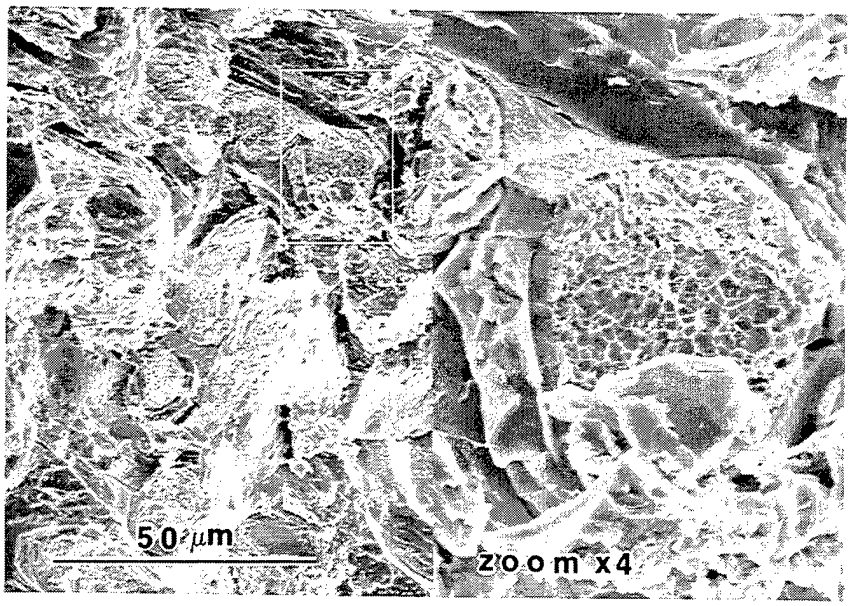


(a)

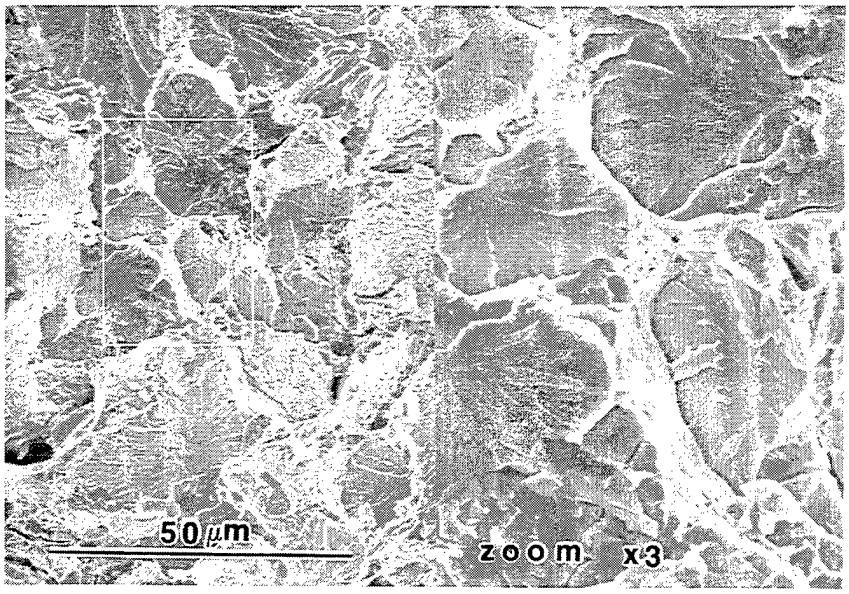


(b)

Figure 21: Fractographs of the twice-extruded (E2) Nb-10 a/o Si alloy tested in four-point bending at room temperature. (a) A primary Nb particle that has debonded from the $Nb_3Si$ matrix and undergone ductile failure. (b) A polycrystalline primary Nb particle which shows cleavage failure over a part of the grains, and ductile ridges along the grain boundaries.

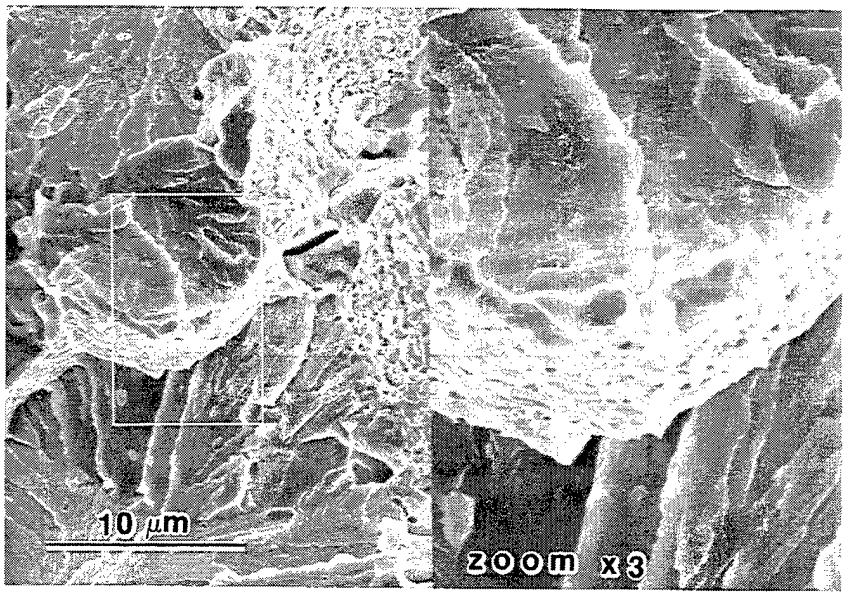


(c)

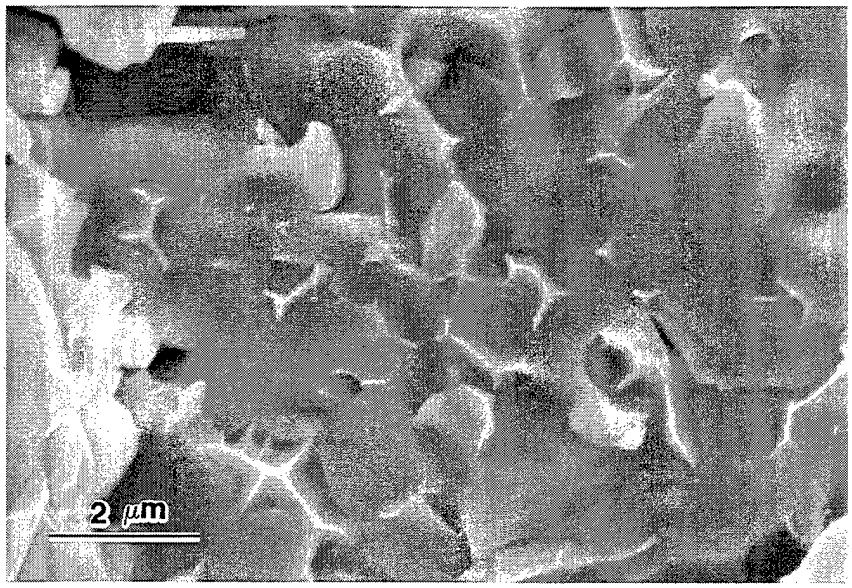


(d)

Figure 21: (cont.) (c) The ductile ridge exhibits dimpled failure. (d) The $Nb_3Si$ matrix shows facetted cleavage, and the secondary Nb particles have all been pulled to wedges.

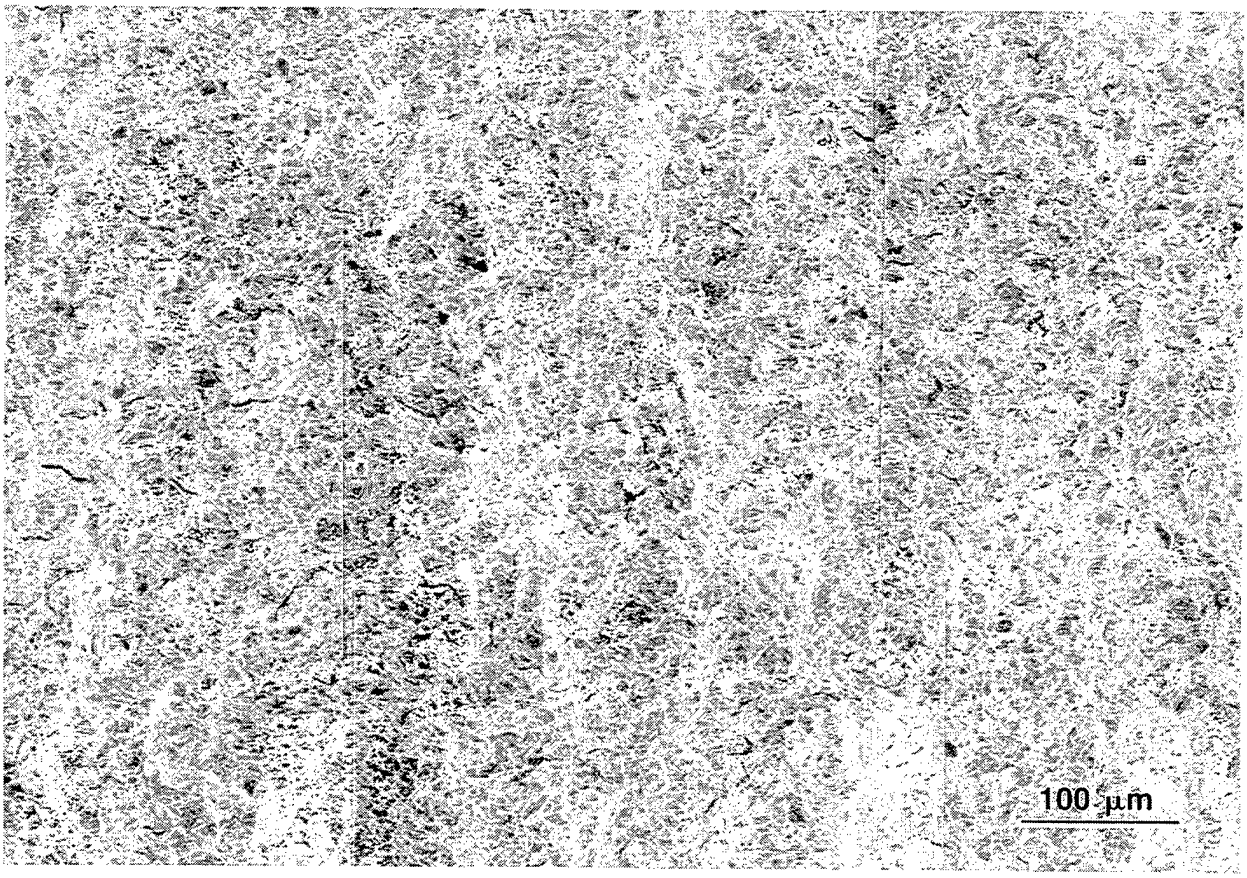


Figure 22: Fracture surface of a notched specimen of the twice-extruded (E2) Nb-10 a/o Si alloy tested in four-point bending at 1000°C. All the primary Nb particles have failed in a ductile manner. The $Nb_3Si$ matrix exhibits extensive microcracking.

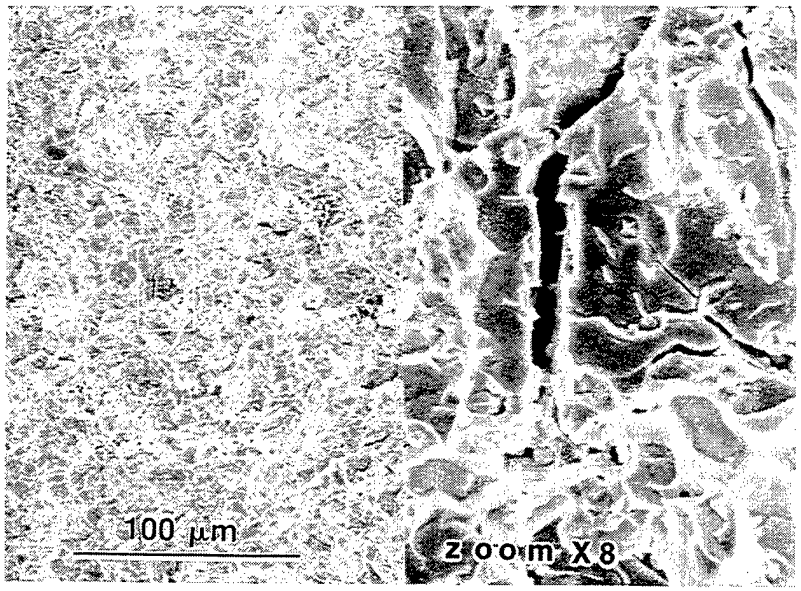


Figure 23: A region of the fracture surface shown in Figure 22. The primary and secondary Nb particles have undergone ductile failure, while the $Nb_3Si$ matrix shown several microcracks.

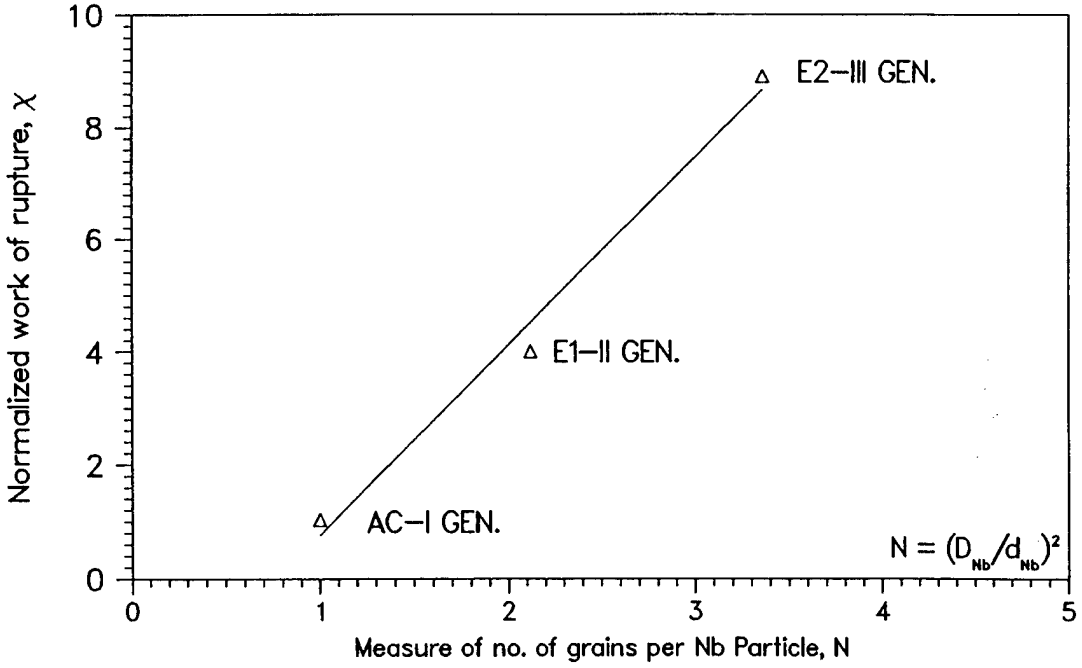


Figure 24: The work of rupture parameter $\chi$ as a function of the number of grains per primary Nb particle.